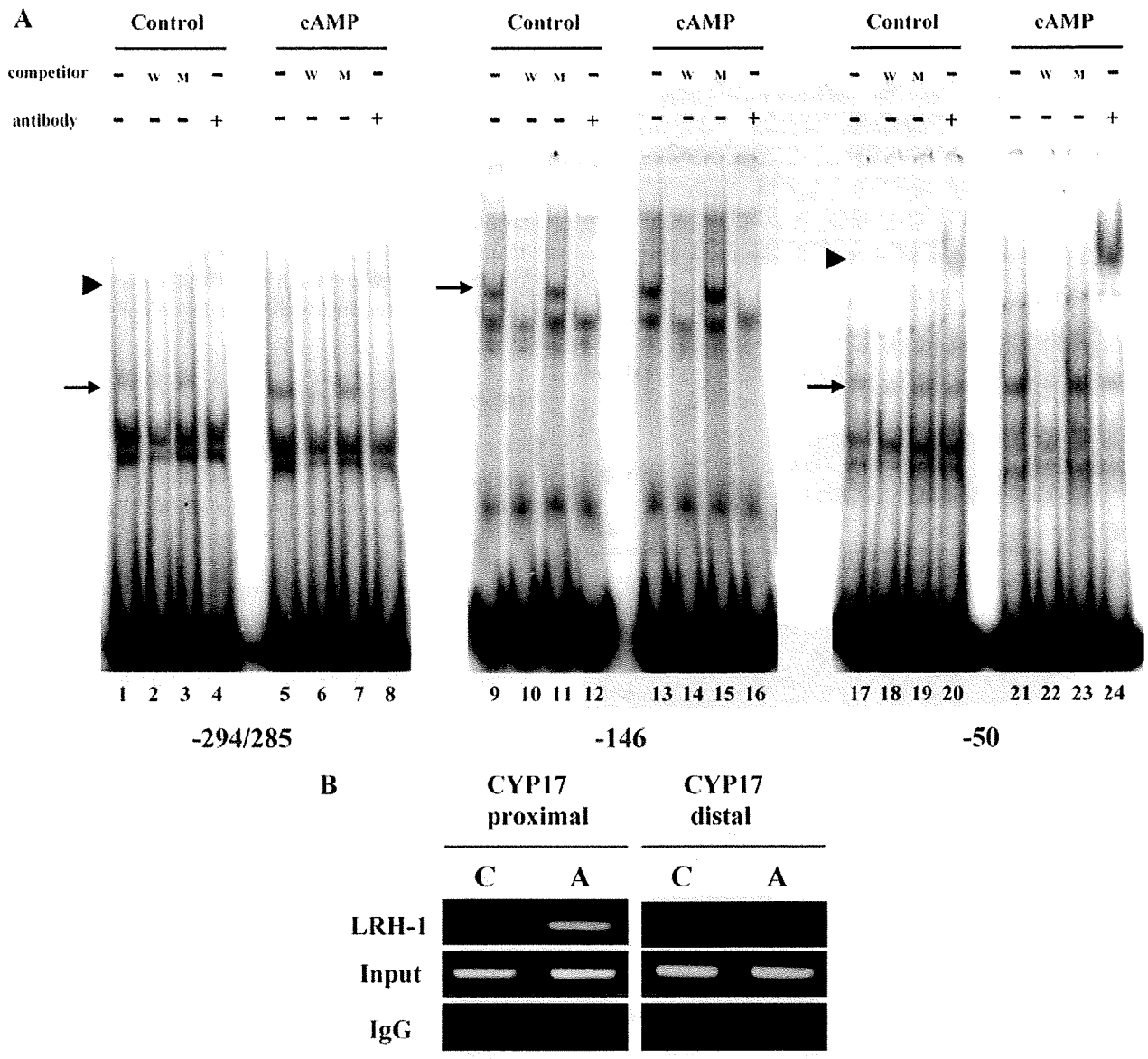

FIG. 4. A, EMSA analyses using Ad4/SF-1-binding sites of CYP17 promoter. Each end-labeled oligonucleotide was incubated with 10 μg of nuclear extracts from cAMP-treated (cAMP; lanes 5–8, 13–16, and 21–24) or cAMP-untreated (control; lanes 1–4, 9–12, and 17–20) LRH-1-transduced hMSCs and resolved by electrophoresis on a nondenaturing 4% (−294/−285 and −50) or 6% (−146) polyacrylamide gel. Wild-type (W; lanes 2, 6, 10, 14, 18, and 22) or mutant (M; lanes 3, 7, 11, 15, 19, and 23) unlabeled oligonucleotides (200-fold molar excess) were used as competitor DNAs. Where indicated (+), antiserum-specific for LRH-1 (lanes 4, 8, 12, 16, 20, 24) was included in the binding reaction. *Arrows* indicate the specific DNA-protein complexes. *Arrowheads* indicate the supershifted complexes. B, ChIP assays were carried out using immunoprecipitated chromatin with IgG or anti-LRH from cAMP-treated (A) or cAMP-untreated (C) LRH-1-transduced hMSCs. Recovered chromatin was subjected to PCR analysis using primers encompassing the LRH-1-binding sites (CYP17 proximal) or approximately 5 kb upstream of the proximal promoter region (CYP17 distal). Data shown are representative of three independent experiments.

or without cAMP were prepared for use in gel mobility shift assays. As shown in Fig. 4, a probe containing each Ad4/SF-1/LRH-1 binding site formed shifted complexes (*arrows*, lanes 1, 5, 9, 13, 17, and 21) that were competed for by each unlabeled oligonucleotide containing homologous sequences (lanes 2, 6, 10, 14, 18, and 22) but not by unlabeled nucleotides containing the mutated sequences that were used for site-directed mutagenesis (lanes 3, 7, 11, 15, 19, and 23). Preincubation of the nuclear extracts with a polyclonal antiserum against LRH-1 shifted (*arrowhead*, lanes 4, 8, 20, and 24) or abolished (lanes 12 and 16) the complex. The intensities of the complex bands were increased after cAMP treatment. ChIP analysis also revealed that the induction of the CYP17 gene by LRH-1 was mediated through direct binding to its promoter region (Fig. 4B). Collectively, these results demonstrated that the CYP17 gene could be a direct target of LRH-1 in human steroidogenic cells.

DNA in the CYP17 promoter is demethylated by cAMP treatment in LRH-1-transduced hMSCs

As we previously reported in adult Leydig-like cells derived from SF-1-transfected murine MSCs (9), there was a time lag associated with the induction of steroidogenic enzymes by camp treatment in LRH-1-transduced hMSCs. P450scc and HSD3B2 mRNAs were rapidly induced within 6–12 h (Fig. 5A). This

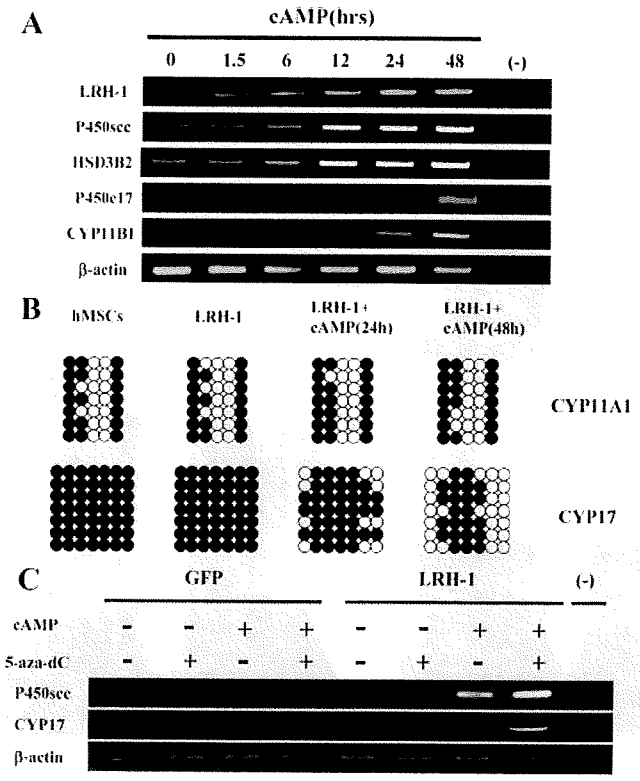

FIG. 5. A, Time-dependent induction of steroidogenic genes by cAMP in hMSCs. LRH-1-transduced hMSCs were cultured and treated with 8-bromo-cAMP (1 mM) for the indicated times. mRNA levels of each gene were analyzed by RT-PCR. B, Analyses of the promoter region of steroidogenic enzymes in nonsteroidogenic hMSCs and steroidogenic hMSCs. Bisulfite genomic sequencing of the promoter region of CYP11A1 and CYP17 in parental hMSCs and LRH-1-transduced hMSCs. LRH-1-transduced cells were treated with 8-bromoadenosine-cAMP (1 mM) for indicated times. *Open* and *closed circles* indicate unmethylated or methylated CpG, respectively. C, Effects of 5aza-dC on the expression of steroidogenic genes. Shown are RT-PCR analyses of each gene in cells cultured with or without cAMP (1 mM) for 18 h after the treatment with 5-aza-dC (25 μM) for 3 d.

pattern is very similar to that of LRH-1 mRNA induction. CYP17 and CYP11B1, however, were induced only after 24–48 h, much later than the induction of LRH-1.

In addition to transcriptional regulation by transcription factors, epigenetic modifications also contribute to the regulation of gene expression. Among them, DNA methylation at cytosine residues of the dinucleotide sequence CpG induces gene silencing and is essential for differentiation and development (35, 36). To compare the DNA methylation status of the steroidogenic genes induced at different times, bisulfite sequencing analysis was performed on the CYP11A1 (the gene encoding P450scc) and CYP17 promoter regions in hMSCs (Fig. 5B). CYP11A1 promoter regions were comparatively hypomethylated in parental hMSCs and GFP-transduced cells (data not shown). This condition was almost completely unchanged by LRH-1 transduction and cAMP treatment. In contrast, CYP17 promoter regions were completely methylated in parental hMSCs. Transduction by LRH-1 had no effect, as in the case of the CYP11A1 promoter. However, cAMP treatment mosaically demethylated the CYP17 promoter regions at 24 h and demethylation was increased by 48 h. These methylation patterns of the CYP11A1 and CYP17 promoters closely paralleled the induction patterns of both genes by cAMP. To clarify the potential role of DNA methylation in the expression of steroidogenic enzymes in hMSCs, LRH-1-transduced cells were treated with the demethylating agent, 5-aza-2′-deoxycytidine (5-aza-dC) (supplemental Fig. 3 and Fig. 5C). Although 5-aza-dC was unable to induce CYP11A1 and CYP17 genes, it augmented the induction of both genes by cAMP, with the effect on CYP17 being particularly marked. These results strongly suggest that the status of DNA methylation in the promoter regions could be important for regulating the expression of steroidogenic enzymes in MSCs and might be responsible for the time lag associated with the induction of some genes.

Discussion

SF-1 has been clearly demonstrated to be a master regulator of steroidogenic organs. SF-1 knockout mice show agenesis of the primary steroidogenic organs, the adrenals and gonads (5–8). SF-1 can induce the differentiation of nonsteroidogenic MSCs into steroidogenic cells (9, 10, 37, 38). In this study, we demonstrated that LRH-1 could also act as a key regulator of the steroidogenic lineage. It was abundant in the gonads and induced the differentiation of MSCs into steroidogenic cells without SF-1. Consistent with our results, it has been reported that LRH-1 and SF-1 have similar roles in steroidogenesis in some cells (20, 39). The analysis of LRH-1 actions *in vivo* has been hampered by the embryonic lethality of LRH-1 knockout mice, although steroidogenesis in heterozygous Lrh-$1^{+/-}$ mice was abnormal in various organs such as the testis, luteinized ovary, and intestine (20, 22–24). Moreover, it was recently reported that ovarian progesterone production was reduced in mice lacking LRH-1 in the granulosa cells (19). It is therefore possible that LRH-1, as well as SF-1, is important for adult steroidogenesis *in vivo*. In addition to detailed analysis of steroidogenesis in the adult, the generation and characterization of mice deficient for LRH-1 in their steroidogenic organs will also help to elucidate its involvement in the development of steroidogenic organs. In fact, granulosa cell-specific knockout model demonstrate a broader role for LRH-1 beyond steroidogenesis in these cells, such as the failure of luteinization (19).

LRH-1-transduced cells abundantly expressed CYP17 and produced testosterone with the aid of cAMP. In human steroidogenic organs, LRH-1 and CYP17 were colocalized in testicular Leydig cells. It is therefore possible that LRH-1 is involved in testicular androgen production. In accordance with our results, Volle *et al.* (20) reported that LRH-$1^{+/-}$ mice showed lower plasma testosterone concentrations than LRH-$1^{+/+}$ mice. However, even though the testicular mRNA levels of various steroidogenic genes such as Star, Cyp11a1, and Hsd3b1 were lower in LRH-$1^{+/-}$ mice, there were no differences in the expression of the Cyp17 gene between LRH-$1^{+/+}$ and LRH-$1^{+/-}$ mice. Deletion of SHP, a transcriptional repressor of LRH-1, however, resulted in increased testosterone production due to enhanced expression of StAR, Cyp11a1, and Hsd3b1. In these mice, the testicular expression of Cyp17 was unaffected. The authors therefore concluded that expression of the Cyp17 gene might not be controlled by the LRH-1/SHP pathway. Our study, however,

clearly demonstrated that LRH-1 directly regulated the transcription of the CYP17 gene via three binding sites located in its promoter region. There are several possible explanations for the discrepancies between these results: it is possible that the regulation of CYP17/Cyp17 gene transcription by the NR5A family varies between species, and Miller and his colleagues (40) noted species-specific variation in the transcriptional regulatory strategies of the CYP17 gene. Observations made in one species cannot therefore reliably be applied to the CYP17 gene in another species, despite the high-sequence similarity of their promoter regions. Another possibility is that although LRH-1 could regulate the transcription of the Cyp17 gene in mouse Leydig cells, haploinsufficiency might be compensated for by other factors, such as SF-1. It is also possible that it could be compensated for by factor(s) derived from other cells by the reduction of LRH-1. Studies in a Leydig cell-specific knockout model would resolve these issues and clarify the role of LRH-1 in androgen production in adult Leydig cells. On the other hand, LRH-1 is unlikely to be involved in steroidogenesis in the fetal testis because it was not detectable in the interstitial space in fetuses or neonates, when the fetal Leydig cells are responsible for the production of testicular androgens (data not shown). In addition, our stem cell model used in this study could also contribute to the investigation of LRH-1 function in steroidogenesis because hMSCs differentiated into SF-1-deficient steroidogenic cells.

Its expression in spermatogenic cells indicates that, in addition to its role in androgen synthesis, LRH-1 could also play a vital role in human spermatogenesis. Expression of LRH-1 has also been reported in both Leydig cells and spermatogenic cells in rats (41). Its localization was similar to the spatial pattern of expression of the aromatase gene in the testis, leading to the suggestion that LRH-1 might regulate the expression of the aromatase gene in not only Leydig cells but also spermatogenic cells and so be involved in intratesticular estrogen signaling. This hypothesis is consistent with the results in MSCs (Fig. 1), in which aromatase was induced by the introduction of LRH-1, aided by cAMP signaling. On the other hand, ovarian aromatase expression was increased in granulosa cell-specific knockout. The results of ChIP analysis indicated that ovarian aromatase expression was not regulated by LRH-1. Hence, the regulation of aromatase gene expression might be complex. In addition to aromatase, LRH-1 could also regulate other genes associated with spermatogenesis in spermatogenic cells.

In addition to steroidogenic enzymes, SF-1 and LRH-1 mRNAs were also induced by cAMP treatment in their respectively transduced cells. Hormone/cAMP regulation of SF-1 and LRH-1 remains a debatable subject because results have varied, depending on the cells used. Similar phenomena to those seen in this study were observed in relatively undifferentiated adrenocortical cell lines stimulated with ACTH (42). However, it has been shown in Leydig or adrenocortical cell lines that SF-1 mRNA levels were largely unaffected by LH/human chorionic gonadotropin, ACTH, or agents that stimulated cAMP production (43–45). Although the reasons for this apparent discrepancy remain unclear, the expression of SF-1 in granulosa cells derived from diethylstilbestrol-primed rats may indicate the complex pattern needed to explain the differences between cells (29). In this model, SF-1 mRNA and protein levels remained almost constant for at least 4 h after FSH treatment but then increased markedly from 12 to 24 h and up to 48 h. This pattern parallels that of the induction of steroidogenic genes and steroidogenesis (luteinization). Once luteinized, SF-1 levels in granulosa cells were unaffected by human chorionic gonadotropin or cAMP treatment, even though progesterone production was increased by these treatments (46). Thus, SF-1 or LRH-1 might be up-regulated during the differentiation of steroidogenic cells by a pituitary hormone/cAMP pathway. However, their expressions should be unaffected after differentiation has occurred. In support of this hypothesis, SF-1 proteins were also induced in nonsteroidogenic Leydig stem cells when they were cultured in medium containing LH and differentiated into testosterone-producing cells (47). As described above, SF-1 was not responsive to the LH/cAMP pathway in differentiated Leydig cells (43–45). Although the precise mechanism underlying the up-regulation of SF-1 and LRH-1 mRNA by cAMP signaling is not clear, mRNA stabilization of both genes is likely to be responsible for this up-regulation; mRNA levels of other genes (GFP, DAX-1, and NUR77) transduced into hMSCs using the same retrovirus vector (same promoter) were not affected by cAMP treatment. Further studies are necessary to determine the mechanisms of NR5A-regulated expression.

Bisulfite sequencing analysis demonstrated that the CYP17 promoter was completely methylated in hMSCs and was demethylated by LRH-1 transduction and cAMP treatment. In contrast to the CYP17 gene, the CYP11A1 promoter region was relatively hypomethylated and was unaffected by LRH-1 and cAMP. It has been shown that methylation of the CpG site in the promoter region was involved in the silencing of tissue-specific genes (48, 49). Consistent with this fact, the methylation patterns of the CYP11A1 and CYP17 promoters closely paralleled the expression patterns of both genes. Low levels of P450scc mRNA were expressed in LRH-1-transduced cells before cAMP treatment, whereas CYP17 mRNAs were expressed after 24 h and only after cAMP treatment. Treatment with the demethylating agent 5-aza-dC up-regulated CYP17 mRNA. These results suggest that DNA methylation is an important determinant of the timing of induction of steroidogenic genes in MSC-derived steroidogenic cells. Similar results were obtained from SF-1-transduced MSCs (our unpublished results). Although the mechanisms of demethylation of the CYP17 promoter region by NR5A family and cAMP were not determined, it has been reported that cyclical changes in the methylation status of promoter CpG islands, mediated by DNA methyltransferases, occurred in genes regulated by the estrogen receptor and its ligand (50, 51). A similar phenomenon might occur in genes regulated by LRH-1 and SF-1, which is also a nuclear receptor. Further studies are necessary to elucidate the mechanisms involved in the regulation of the methylation states of steroidogenic genes in MSCs.

In summary, we have determined that LRH-1, as well as SF-1, could act as a key regulator controlling the differentiation of some stem cells into steroidogenic cells. It is possible that the function of SF-1 in primary steroidogenesis could be replaced by LRH-1. In support of this hypothesis, Ingraham and her colleagues (52) showed, using SF-1 haploinsufficient mice, that the

full SF-1 gene dosage was necessary for early adrenal development but not in the adult adrenal, in which compensatory mechanisms restored near normal function. In addition, Morohashi and his colleagues (8, 53), using transgenic mice, reported that differential gene dosage effects of SF-1/Ad4BP existed between the gonads and adrenals, even though they had a common developmental origin. Our results strongly suggest that LRH-1 is involved in these phenomena and can compensate for SF-1 function in these models. Future studies aimed at simultaneously investigating the functions of both SF-1 and LRH-1 will be essential for developing a more precise understanding of the regulation of primary steroidogenesis.

Acknowledgments

We thank Drs. K. Morohashi, J. Toguchida, L. Bèlanger, A. J. Conley, and J. I. Mason for providing materials. We thank Dr. T. Sekiguchi for critical reading of the manuscript. We also thank Ms. Y. Inoue, Y. Yamazaki, M. Uesaka, K. Matsuura, and H. Fujii for technical assistance.

Address all correspondence and requests for reprints to: Professor Kaoru Miyamoto, Department of Biochemistry, Faculty of Medical Sciences, University of Fukui, Shimoaizuki, Matsuoka, Eiheiji-cho, Fukui 910-1193 Japan. E-mail: kmiyamot@u-fukui.ac.jp.

This work was supported by a grant from the Ministry of Education, Culture, Sports, Science, and Technology of Japan and the Smoking Research Foundation.

Disclosure Summary: The authors have nothing to disclose.

References

1. Krylova IN, Sablin EP, Moore J, Xu RX, Waitt GM, MacKay JA, Juzumiene D, Bynum JM, Madauss K, Montana V, Lebedeva L, Suzawa M, Williams JD, Williams SP, Guy RK, Thornton JW, Fletterick RJ, Willson TM, Ingraham HA 2005 Structural analyses reveal phosphatidyl inositols as ligands for the NR5 orphan receptors SF-1 and LRH-1. Cell 120:343–355
2. Lala DS, Rice DA, Parker KL 1992 Steroidogenic factor I, a key regulator of steroidogenic enzyme expression, is the mouse homolog of fushi tarazu-factor I. Mol Endocrinol 6:1249–1258
3. Morohashi K, Honda S, Inomata Y, Handa H, Omura T 1992 A common trans-acting factor, Ad4-binding protein, to the promoters of steroidogenic P-450s. J Biol Chem 267:17913–17919
4. Galarneau L, Paré JF, Allard D, Hamel D, Levesque L, Tugwood JD, Green S, Bélanger L 1996 The α1-fetoprotein locus is activated by a nuclear receptor of the Drosophila FTZ-F1 family. Mol Cell Biol 16:3853–3865
5. Luo X, Ikeda Y, Parker KL 1994 A cell-specific nuclear receptor is essential for adrenal and gonadal development and sexual differentiation. Cell 77:481–490
6. Sadovsky Y, Crawford PA, Woodson KG, Polish JA, Clements MA, Tourtellotte LM, Simburger K, Milbrandt J 1995 Mice deficient in the orphan receptor steroidogenic factor 1 lack adrenal glands and gonads but express P450 side-chain-cleavage enzyme in the placenta and have normal embryonic serum levels of corticosteroids. Proc Natl Acad Sci USA 92:10939–10943
7. Parker KL, Schimmer BP 1997 Steroidogenic factor 1: a key determinant of endocrine development and function. Endocr Rev 18:361–377
8. Morohashi Ki 1999 Gonadal and extragonadal functions of Ad4BP/SF-1: developmental aspects. Trends Endocrinol Metab 10:169–173
9. Yazawa T, Mizutani T, Yamada K, Kawata H, Sekiguchi T, Yoshino M, Kajitani T, Shou Z, Umezawa A, Miyamoto K 2006 Differentiation of adult stem cells derived from bone marrow stroma into Leydig or adrenocortical cells. Endocrinology 147:4104–4111
10. Yazawa T, Uesaka M, Inaoka Y, Mizutani T, Sekiguchi T, Kajitani T, Kitano T, Umezawa A, Miyamoto K 2008 Cyp11b1 is induced in the murine gonad by luteinizing hormone/ human chorionic gonadotropin and involved in the production of 11-ketotestosterone, a major fish androgen; conservation and evolution of androgen metabolic pathway. Endocrinology 149:1786–1792
11. Fayard E, Auwerx J, Schoonjans K 2004 LRH-1: an orphan nuclear receptor involved in development, metabolism and steroidogenesis. Trends Cell Biol 14:250–260
12. Lee YK, Moore DD 2008 Liver receptor homolog-1, an emerging metabolic modulator. Front Biosci 13:5950–5958
13. Gu P, Goodwin B, Chung AC, Xu X, Wheeler DA, Price RR, Galardi C, Peng L, Latour AM, Koller BH, Gossen J, Kliewer SA, Cooney AJ 2005 Orphan nuclear receptor LRH-1 is required to maintain Oct4 expression at the epiblast stage of embryonic development. Mol Cell Biol 25:3492–3505
14. Labelle-Dumais C, Jacob-Wagner M, Paré JF, Bélanger L, Dufort D 2006 Nuclear receptor NR5A2 is required for proper primitive streak morphogenesis. Dev Dyn 235:3359–3369
15. Lu TT, Makishima M, Repa JJ, Schoonjans K, Kerr TA, Auwerx J, Mangelsdorf DJ 2000 Molecular basis for feedback regulation of bile acid synthesis by nuclear receptors. Mol Cell 6:507–515
16. Goodwin B, Jones SA, Price RR, Watson MA, McKee DD, Moore LB, Galardi C, Wilson JG, Lewis MC, Roth ME, Maloney PR, Willson TM, Kliewer SA 2000 A regulatory cascade of the nuclear receptors FXR, SHP-1, and LRH-1 represses bile acid biosynthesis. Mol Cell 6:517–526
17. Lee YK, Schmidt DR, Cummins CL, Choi M, Peng L, Zhang Y, Goodwin B, Hammer RE, Mangelsdorf DJ, Kliewer SA 2008 Liver receptor homolog-1 regulates bile acid homeostasis but is not essential for feedback regulation of bile acid synthesis. Mol Endocrinol 22:1345–1356
18. Mataki C, Magnier BC, Houten SM, Annicotte JS, Argmann C, Thomas C, Overmars H, Kulik W, Metzger D, Auwerx J, Schoonjans K 2007 Compromised intestinal lipid absorption in mice with a liver-specific deficiency of liver receptor homolog 1. Mol Cell Biol 27:8330–8339
19. Duggavathi R, Volle DH, Mataki C, Antal MC, Messaddeq N, Auwerx J, Murphy BD, Schoonjans K 2008 Liver receptor homolog 1 is essential for ovulation. Genes Dev 22:1871–1876
20. Volle DH, Duggavathi R, Magnier BC, Houten SM, Cummins CL, Lobaccaro JM, Verhoeven G, Schoonjans K, Auwerx J 2007 The small heterodimer partner is a gonadal gatekeeper of sexual maturation in male mice. Genes Dev 21:303–315
21. Saxena D, Escamilla-Hernandez R, Little-Ihrig L, Zeleznik AJ 2007 Liver receptor homolog-1 and steroidogenic factor-1 have similar actions on rat granulosa cell steroidogenesis. Endocrinology 148:726–734
22. Labelle-Dumais C, Paré JF, Bélanger L, Farookhi R, Dufort D 2007 Impaired progesterone production in Nr5a2$^{+/-}$ mice leads to a reduction in female reproductive function. Biol Reprod 77:217–225
23. Mueller M, Cima I, Noti M, Fuhrer A, Jakob S, Dubuquoy L, Schoonjans K, Brunner T 2006 The nuclear receptor LRH-1 critically regulates extra-adrenal glucocorticoid synthesis in the intestine. J Exp Med 203:2057–2062
24. Coste A, Dubuquoy L, Barnouin R, Annicotte JS, Magnier B, Notti M, Corazza N, Antal MC, Metzger D, Desreumaux P, Brunner T, Auwerx J, Schoonjans K 2007 LRH-1-mediated glucocorticoid synthesis in enterocytes protects against inflammatory bowel disease. Proc Natl Acad Sci USA 104:13098–13103
25. Mueller M, Atanasov A, Cima I, Corazza N, Schoonjans K, Brunner T 2007 Differential regulation of glucocorticoid synthesis in murine intestinal epithelial versus adrenocortical cell lines. Endocrinology 148:1445–1453
26. Mori T, Kiyono T, Imabayashi H, Takeda Y, Tsuchiya K, Miyoshi S, Makino H, Matsumoto K, Saito H, Ogawa S, Sakamoto M, Hata J, Umezawa A 2005 Combination of hTERT and bmi-1, E6, or E7 induces prolongation of the life span of bone marrow stromal cells from an elderly donor without affecting their neurogenic potential. Mol Cell Biol 25:5183–5195
27. Okamoto T, Aoyama T, Nakayama T, Nakamata T, Hosaka T, Nishijo K, Nakamura T, Kiyono T, Toguchida J 2002 Clonal heterogeneity in differentiation potential of immortalized human mesenchymal stem cells. Biochem Biophys Res Commun 295:354–361
28. Yazawa T, Nakayama Y, Fujimoto K, Matsuda Y, Abe K, Kitano T, Abé S, Yamamoto T 2003 Abnormal spermatogenesis at low temperatures in the Japanese red-bellied newt, *Cynops pyrrhogaster*: possible biological significance of the cessation of spermatocytogenesis. Mol Reprod Dev 66:60–66
29. Yazawa T, Mizutani T, Yamada K, Kawata H, Sekiguchi T, Yoshino M, Kajitani T, Shou Z, Miyamoto K 2003 Involvement of cyclic adenosine 5′-monophosphate response element-binding protein, steroidogenic factor 1, and Dax-1 in the regulation of gonadotropin-inducible ovarian transcription factor 1 gene expression by follicle-stimulating hormone in ovarian granulosa cells. Endocrinology 144:1920–1930
30. Hanley NA, Rainey WE, Wilson DI, Ball SG, Parker KL 2001 Expression profiles of SF-1, DAX1, and CYP17 in the human fetal adrenal gland: potential interactions in gene regulation. Mol Endocrinol 15:57–68
31. Sewer MB, Nguyen VQ, Huang CJ, Tucker PW, Kagawa N, Waterman MR 2002 Transcriptional activation of human CYP17 in H295R adrenocortical

cells depends on complex formation among p54(nrb)/NonO, protein-associated splicing factor, and SF-1, a complex that also participates in repression of transcription. Endocrinology 143:1280–1290
32. Lalli E, Sassone-Corsi P 2003 DAX-1, an unusual orphan receptor at the crossroads of steroidogenic function and sexual differentiation. Mol Endocrinol 17:1445–1453
33. Wilson TE, Mouw AR, Weaver CA, Milbrandt J, Parker KL 1993 The orphan nuclear receptor NGFI-B regulates expression of the gene encoding steroid 21-hydroxylase. Mol Cell Biol 13:861–868
34. Peng N, Kim JW, Rainey WE, Carr BR, Attia GR 2003 The role of the orphan nuclear receptor, liver receptor homologue-1, in the regulation of human corpus luteum 3β-hydroxysteroid dehydrogenase type II. J Clin Endocrinol Metab 88:6020–6028
35. Li E, Bestor TH, Jaenisch R 1992 Targeted mutation of the DNA methyltransferase gene results in embryonic lethality. Cell 69:915–926
36. Ng RK, Gurdon JB 2008 Epigenetic inheritance of cell differentiation status. Cell Cycle 7:1173–1177
37. Gondo S, Yanase T, Okabe T, Tanaka T, Morinaga H, Nomura M, Goto K, Nawata H 2004 SF-1/Ad4BP transforms primary long-term cultured bone marrow cells into ACTH-responsive steroidogenic cells. Genes Cells 9:1239–1247
38. Tanaka T, Gondo S, Okabe T, Ohe K, Shirohzu H, Morinaga H, Nomura M, Tani K, Takayanagi R, Nawata H, Yanase T 2007 Steroidogenic factor 1/adrenal 4 binding protein transforms human bone marrow mesenchymal cells into steroidogenic cells. J Mol Endocrinol 39:343–350
39. Wang ZN, Bassett M, Rainey WE 2001 Liver receptor homologue-1 is expressed in the adrenal and can regulate transcription of 11β-hydroxylase. J Mol Endocrinol 27:255–258
40. Lin CJ, Martens JW, Miller WL 2001 NF-1C, Sp1, and Sp3 are essential for transcription of the human gene for P450c17 (steroid 17α-hydroxylase/17,20 lyase) in human adrenal NCI-H295A cells. Mol Endocrinol 15:1277–1293
41. Pezzi V, Sirianni R, Chimento A, Maggiolini M, Bourguiba S, Delalande C, Carreau S, Andò S, Simpson ER, Clyne CD 2004 Differential expression of steroidogenic factor-1/adrenal 4 binding protein and liver receptor homolog-1 (LRH-1)/fetoprotein transcription factor in the rat testis: LRH-1 as a potential regulator of testicular aromatase expression. Endocrinology 145:2186–2196
42. Ragazzon B, Lefrançois-Martinez AM, Val P, Sahut-Barnola I, Tournaire C, Chambon C, Gachancard-Bouya JL, Begue RJ, Veyssière G, Martinez A 2006 Adrenocorticotropin-dependent changes in SF-1/DAX-1 ratio influence steroidogenic genes expression in a novel model of glucocorticoid-producing adrenocortical cell lines derived from targeted tumorigenesis. Endocrinology 147:1805–1818
43. Zhang P, Mellon SH 1996 The orphan nuclear receptor steroidogenic factor-1 regulates the cyclic adenosine 3′,5′-monophosphate-mediated transcriptional activation of rat cytochrome P450c17 (17α-hydroxylase/c17–20 lyase). Mol Endocrinol 10:147–158
44. Jo Y, Stocco DM 2004 Regulation of steroidogenesis and steroidogenic acute regulatory protein in R2C cells by DAX-1 (dosage-sensitive sex reversal, adrenal hypoplasia congenita, critical region on the X chromosome, gene-1). Endocrinology 145:5629–5637
45. Chau YM, Crawford PA, Woodson KG, Polish JA, Olson LM, Sadovsky Y 1997 Role of steroidogenic-factor 1 in basal and 3′,5′-cyclic adenosine monophosphate-mediated regulation of cytochrome P450 side-chain cleavage enzyme in the mouse. Biol Reprod 57:765–771
46. Mamluk R, Greber Y, Meidan R 1999 Hormonal regulation of messenger ribonucleic acid expression for steroidogenic factor-1, steroidogenic acute regulatory protein, and cytochrome P450 side-chain cleavage in bovine luteal cells. Biol Reprod 60:628–634
47. Ge RS, Dong Q, Sottas CM, Papadopoulos V, Zirkin BR, Hardy MP 2006 In search of rat stem Leydig cells: identification, isolation, and lineage-specific development. Proc Natl Acad Sci USA 103:2719–2724
48. Eden S, Cedar H 1994 Role of DNA methylation in the regulation of transcription. Curr Opin Genet Dev 4:255–259
49. Xue Q, Lin Z, Yin P, Milad MP, Cheng YH, Confino E, Reierstad S, Bulun SE 2007 Transcriptional activation of steroidogenic factor-1 by hypomethylation of the 5′ CpG island in endometriosis. J Clin Endocrinol Metab 92:3261–3267
50. Métivier R, Gallais R, Tiffoche C, Le Péron C, Jurkowska RZ, Carmouche RP, Ibberson D, Barath P, Demay F, Reid G, Benes V, Jeltsch A, Gannon F, Salbert G 2008 Cyclical DNA methylation of a transcriptionally active promoter. Nature 452:45–50
51. Kangaspeska S, Stride B, Métivier R, Polycarpou-Schwarz M, Ibberson D, Carmouche RP, Benes V, Gannon F, Reid G 2008 Transient cyclical methylation of promoter DNA. Nature 452:112–115
52. Bland ML, Fowkes RC, Ingraham HA 2004 Differential requirement for steroidogenic factor-1 gene dosage in adrenal development versus endocrine function. Mol Endocrinol 18:941–952
53. Fatchiyah, Zubair M, Shima Y, Oka S, Ishihara S, Fukui-Katoh Y, Morohashi K 2006 Differential gene dosage effects of Ad4BP/SF-1 on target tissue development. Biochem Biophys Res Commun 341:1036–1045

５マイクロバブルを援用した超音波遺伝子導入

岡本旭生 1、橘理恵 1、葭仲潔 2、高木周 1、松本洋一郎 1

1 東京大学工学系研究科機械工学専攻流体工学研究室、2 東京大学工学系研究科バイオエンジニアリング専攻流体工学研究室【目的】マイクロバブルを援用した超音波遺伝子導入法の開発について報告する。【方法】In vitro においてマウス線維芽細胞系 NIH3T3 に GFP プラスミドを導入する実験を、超音波照射時の条件を変化させて行った。結果、照射する超音波の強度が大きいほど、また超音波の照射時間が長いほど、生き残った細胞中への導入率が大きくなることが示されたが、すべての実験条件において遺伝子導入率が極めて小さいことが判明した。この原因を、細胞生存率の定量化および小孔形成細胞の可視化により解明することを目指した。【結果】細胞生存率定量化の結果、8 割程度の細胞が生存していることがわかった。また、多数の細胞に小孔が形成されていることが明らかになった。【結論】以上の実験結果より、遺伝子導入率が低いことの原因は、細胞内に遺伝子が取り込まれていないこと、あるいは取り込まれた遺伝子が発現していないことであると考察する。

Active Path Selection of Fluid Microcapsules in Artificial Blood Vessel by Acoustic Radiation Force

Kohji Masuda*, Yusuke Muramatsu, Sawami Ueda, Ryusuke Nakamoto, Yusuke Nakayashiki, and Ken Ishihara[1]

Graduate School of Bio-Applications and Systems Engineering, Tokyo University of Agriculture and Technology, 2-24 Nakacho, Koganei, Tokyo 184-8588, Japan
[1]*School of Medicine, Ehime University, Shitsukawa, Toon, Ehime 791-0295, Japan*

Received November 19, 2008; accepted February 25, 2009; published online July 21, 2009

Micrometer-sized microcapsules collapse upon exposure to ultrasound. Use of this phenomenon for a drug delivery system (DDS), not only for local delivery of medication but also for gene therapy, should be possible. However, enhancing the efficiency of medication is limited because capsules in suspension diffuse in the human body after injection, since the motion of capsules in blood flow cannot be controlled. To control the behavior of microcapsules, acoustic radiation force was introduced. We detected local changes in microcapsule density by producing acoustic radiation force in an artificial blood vessel. Furthermore, we theoretically estimated the conditions required for active path selection of capsules at a bifurcation point in the artificial blood vessel. We observed the difference in capsule density at both in the bifurcation point and in alternative paths downstream of the bifurcation point for different acoustic radiation forces. Comparing the experimental results with those obtained theoretically, the conditions for active path selection were calculated from the acoustic radiation force and fluid resistance of the capsules. The possibility of controlling capsule flow towards a specific point in a blood vessel was demonstrated.

DOI: 10.1143/JJAP.48.07GK03

1. Introduction

The phenomenon that microcapsules or microbubbles of micrometer size collapse upon exposure to ultrasound near their resonance frequency has been identified as a basis for a physical drug delivery system (DDS).[1–3] To minimize side effects, medication should only affect the target area, not other parts of the human body. Although the majority of recent research on DDSs has been focused on gene transduction using gene vectors, this method takes time and its development is costly. The microcapsules, which can contain a specific drug inside a shell, are suitable for use with various types of medication. Furthermore, microcapsules are easily detected[4] and actuated[5,6] by ultrasound. The distribution of capsules inside the body is easily determined by echogram (B-mode image) because the brightness of an echogram varies depending on capsule density. We have developed software to detect local changes in capsule density using the variation in brightness of an echogram.[7,8] Figure 1 shows a microscope image of F-80E microcapsules (Matsumoto Oil), which we used in this work.

However, because of the diffusion of capsules after injection, it is difficult to enhance the efficiency of medication. If the behavior of capsules could be controlled, the amount of medication required would be minimized. Microbubbles aggregate in water owing to Bjerknes forces,[9,10] which are produced by an ultrasound pressure gradient and oscillation of the diameter of the microbubbles. Since the oscillation of microcapsules is smaller than that of microbubbles, because of the microcapsule shell, a microcapsule is thought to receive an acoustic radiation force[11,12] and be propelled by acoustic propagation. In this paper, we describe our attempt[13,14] for active path selection of microcapsules in an artificial blood vessel by acoustic radiation force.

2. Theory

Assuming spherical microcapsules, an acoustic radiation force[11] acts to propel the capsules in the direction of acoustic propagation as per the following equation:

$$F_{ac} = \frac{4}{3}\pi {R_0}^3 A \frac{P^2}{\rho c^2}, \tag{1}$$

where R_0 is the average capsule radius, P is the sound pressure, ρ is the density of the medium, and A is a constant.

When the microcapsules are placed in flow, a capsule should receive a flow resistance F_d as per the following equation:

$$F_d = 6\pi R_0 \mu u_r, \tag{2}$$

where u_r is the velocity caused by the acoustic radiation force and μ is the viscosity coefficient of the medium.

Thus, if ultrasound is directed at a microcapsule in flow, and the acoustic radiation force is greater than the flow resistance, the trajectory of the capsule is curved, as shown in Fig. 2.

When microcapsules pass through an acoustic field where the sound pressure is higher than that in other areas, capsules are propelled away from their original course. At larger values of angle θ in Fig. 2, a capsule passes through the acoustic field for a longer period causing a larger displacement from the original course. The displacement of a capsule before it reaches the bifurcation point, shown in Fig. 2, can be calculated using eq. (3), where m is the weight

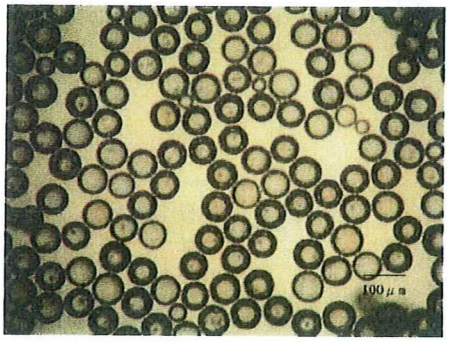

Fig. 1. (Color online) Microscope image of F-80E microcapsules.

*E-mail address: masuda_k@cc.tuat.ac.jp

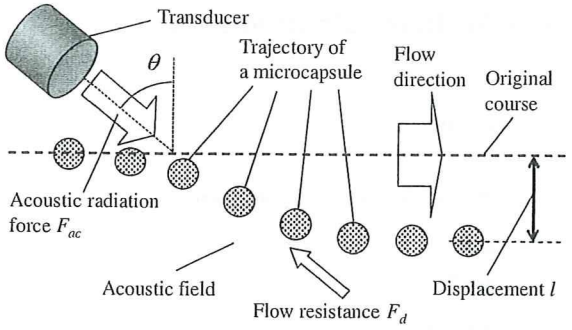

Fig. 2. Trajectory of microcapsule in flow under ultrasound emission.

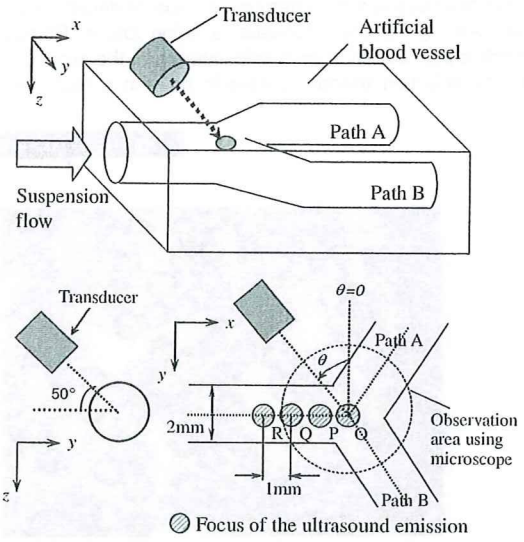

Fig. 3. Schematic view of artificial blood vessel.

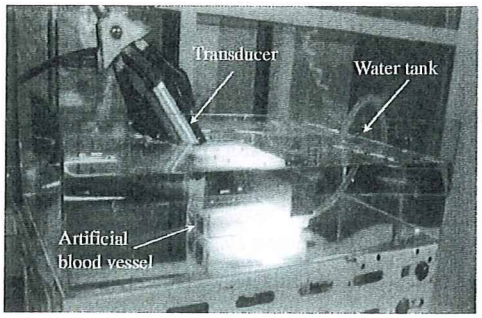

Fig. 4. Configuration of artificial blood vessel, transducer, and water tank.

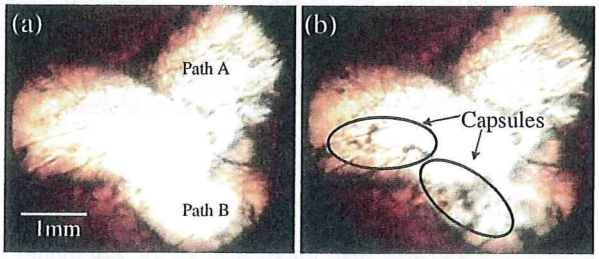

Fig. 5. (Color online) Comparison of microscope images of observation area (a) before and (b) after injection of capsule suspension with ultrasound focused at point Q.

of a capsule. In Fig. 2, although the shape of the acoustic field is expressed as a square, it is dependent upon the transducer and should be measured before the calculation of theoretical displacement.

$$l = \iint \frac{(F_{ac} - F_d)\cos\theta}{m}\, dt\, dt \tag{3}$$

3. Experiments

3.1 Observation of capsule behavior

We used the above-mentioned F-80E microcapsule, which has a shell made of poly(vinyl chloride) (PVC), a specific gravity of 0.0225, and an average diameter of 99.2 μm. We selected only those microcapsules with a diameter in the range from 65 to 73 μm because of the limited magnification of the microscope. This size of capsule, of course, is not suitable for use *in vivo*, but is useful for confirming the fundamental behavior of capsules before minimizing them in future experiments.

We have also prepared an artificial blood vessel made of poly(ethylene glycol) (PEG), including a Y-form bifurcation, as shown in the schematic view of Fig. 3. The external size was $50 \times 80 \times 10\,\mathrm{mm}^3$ and the inner diameter of the paths was 2 mm. The blood vessel was placed in the bottom of a water tank, which was filled with water. Because the acoustic impedance of PEG is similar to that of water, the energy of ultrasound in water reaches the path with high efficiency. Using an inverted microscope (Leica, DMRIB), an optical image of the observation area indicated in Fig. 3 was recorded.

As shown in Fig. 3, the axis of the transducer was set at 50° counterclockwise to the x-axis and θ deg clockwise to the z-axis to prevent physical interference between the transducer and the edge of the water tank. Figure 4 shows the configuration of the experimental setup. The transducer included a concave ceramic disc with a diameter of 25 mm. Ultrasound was emitted by amplifying a sinusoidal signal of 1 MHz to an amplitude of 160 kPa where the focal area of ultrasound is created in 60 mm from the surface of the transducer with a half width of sound pressure of 8 mm.

The center of the focal area is set at the point indicated in Fig. 3. Defining point O as the intersection of the three paths, the points P, Q, and R indicate points 1, 2, and 3 mm upstream from O, respectively. We observed the behavior of capsules near the bifurcation point shown in Fig. 3 upon the injection of a capsule suspension at a flow velocity of 100 mm/s. Floatation of the capsules owing to their buoyancy was not confirmed. When ultrasound was emitted, more capsules entered path B than path A, whereas no significant difference was observed without ultrasound emission. Figure 5 shows the comparison of microscope images of the observation area before and after the capsule suspension was injected and ultrasound was focused at point Q. Since a large amount of capsules was observed as a shadow, the possibility of active path selection of capsules was indicated. Here we confirmed that the capsules were not destroyed by the ultrasound since the frequency used was far from the resonance frequency of the capsules.

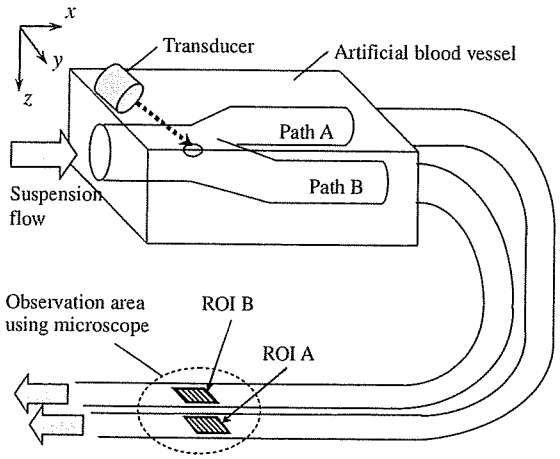

Fig. 6. Observation area for determining number of capsules in each path.

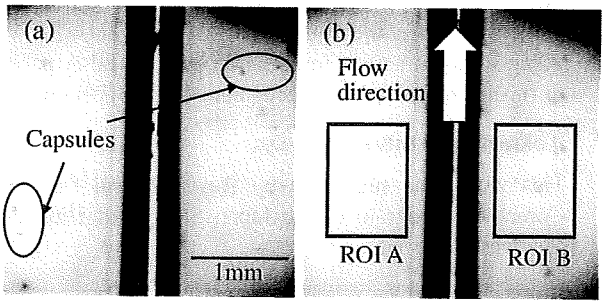

Fig. 7. Microscope images of observation area taken at 500 fps after injection of capsule suspension (a) without and (b) with ultrasound emission.

3.2 Evaluation of path selection

To evaluate the number of capsules that passed through each path, we extended the two paths using semitransparent tubes and established an observation area, where both paths were observable in a single view, as shown in Fig. 6.

Figure 7 shows microscope images of the area, which were captured using a high-speed camera Phantom-V4.2 (Nobitec) with an interval time of 2 ms, upon injection of a capsule suspension under the same conditions as for Fig. 5. Individual microcapsules can be distinguished.

To measure the number of capsules, we established two square regions of interest in each path [region of interests (ROIs) A and B] and calculated the average brightness.[13,14] The brightness of a region decreases depending on the number of capsules present. Thus, we defined the shadow index σ using the following equation to determine the number of capsules in each ROI:

$$\sigma = \frac{REF - \sum_x \sum_y f(x,y)}{REF}, \quad (4)$$

where f is the brightness of the ROI and REF is the summation of brightness in the absence of capsules in the ROI. Then, we confirmed the relationship between shadow index and capsule density. A capsule suspension was passed through the ROI without ultrasound and the average of the

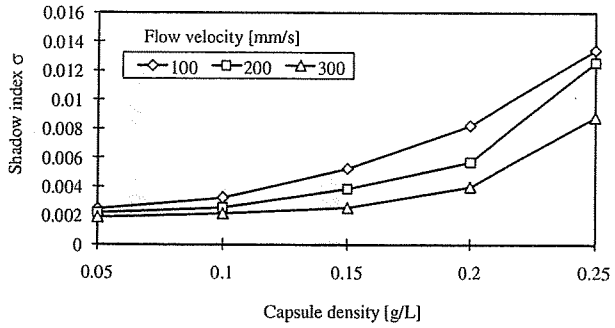

Fig. 8. Shadow index versus capsule density.

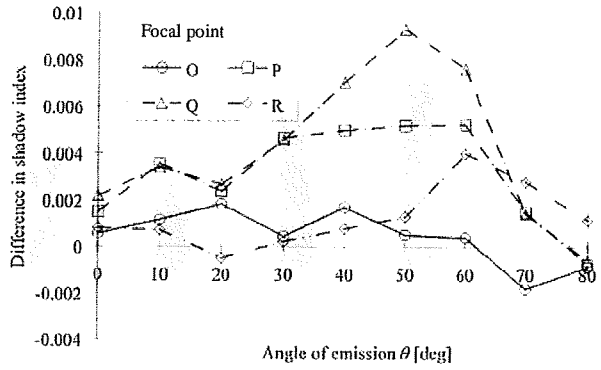

Fig. 9. Shadow index difference between two ROIs versus angle of emission with focused ultrasound of 1 MHz, 160 kPa, and flow velocity of 100 mm/s.

shadow index for 15 frames (duration 30 ms) was calculated for various flow velocities. As shown in Fig. 8, using capsule densities of 0.15–0.25 g/L, significant changes in density were detected.

4. Results and Discussion

We measured the shadow indices in two ROIs upon emission of sinusoidal ultrasound with a frequency of 1 MHz, a flow velocity of 100 mm/s, and a capsule density of 0.2 g/L, where ultrasound was focused at points O, P, Q, and R shown in Fig. 3. Figure 9 shows the difference in shadow indices between ROIs A and B versus the angle of ultrasound emission θ for four focal points. Because the difference was calculated by subtracting the shadow index of ROI A from that of ROI B, a positive value for the difference indicates that more capsules passed through path B than path A. When the focal point was at O, no significant difference was observed. Upstream from O, clear capsule selection to path B was confirmed at angles of emission between 30 and 60°. The optimum condition for active path selection in the experiment was at an angle of 50° at focal point Q, which was used in the following experiment.

We repeated the same experiment at a flow velocity of 100 mm/s. Figure 10 shows the values of shadow indices versus sound pressure. When the sound pressure was less than 120 kPa, there was no difference between the two ROIs. However, the value of shadow index in ROI B increased in proportion to the sound pressure at more than 140 kPa. More than 90% of the capsules entered path B when the sound pressure was more than 160 kPa. In the same figure we show

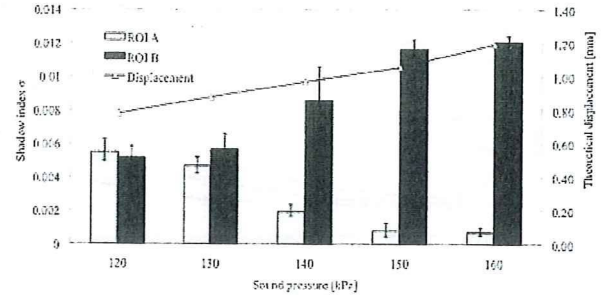

Fig. 10. Shadow indices in two ROIs versus sound pressure with 1 MHz ultrasound focused at point Q and flow velocity of 100 mm/s.

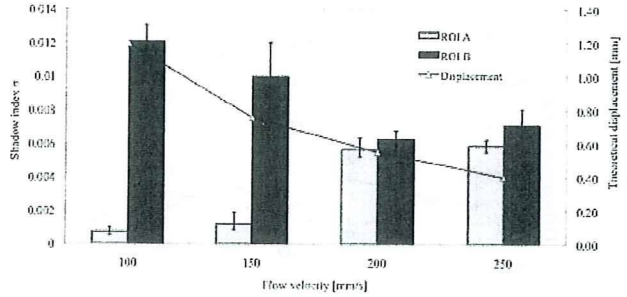

Fig. 11. Shadow indices in two ROIs versus flow velocity with 1 MHz ultrasound focused at point Q and sound pressure of 160 kPa.

the displacement of a capsule, as determined using eq. (3) for the same conditions by assuming an acoustic field width of 3 mm from the half width of the maximum sound pressure. When the sound pressure was between 130 and 140 kPa, the displacement of a capsule should be approximately 1 mm, which is half of the inner diameter of the artificial blood vessel.

Next, we fixed the sound pressure at 160 kPa. Figure 11 shows the values of shadow indices versus flow velocity. The value of shadow index in path B decreased in proportion to the flow velocity. The range of flow velocity for path selection appears to be 150–200 mm/s. When the flow velocity was more than 200 mm/s, path selection did not function, which we assume is because the capsules pass through the acoustic field without receiving sufficient acoustic radiation force. When the flow velocity was 150 mm/s, the theoretical displacement was determined to be 0.7 mm, which is similar to the actual result shown in Fig. 10.

From these results, the sound pressure, focal point, and flow velocity should be considered to realize active path selection of microcapsules. When the focal point of ultrasound emission is at the bifurcation point itself, active path selection of capsules is not realized. The focal point should be located upstream from the bifurcation point to ensure sufficient displacement of capsules. In the present experiment, the inner diameter of the path was 2 mm, so a 1 mm displacement was necessary from the beginning of the acoustic field to the bifurcation point, as shown in Fig. 2. For further analysis, the precise conditions necessary to realize active path selection for more complicated shapes of blood vessel should be elucidated.

5. Conclusions

In this study, we realized active path selection of microcapsules at a bifurcation point in an artificial blood vessel. We confirmed that capsules with a diameter between 65 and 73 μm were directed into the desired path and were not destroyed by ultrasound of a sinusoidal signal of 1 MHz. The conditions for active path selection of capsules were as follows: 1) a sound pressure higher than 150 kPa when the flow velocity was 100 m/s and 2) a flow velocity lower than 150 mm/s when the sound pressure was 160 kPa. We are going to continue our research by varying other parameters to further elucidate the mechanism of this phenomenon.

Acknowledgment

This work was supported by Research and Development Committee Program of the Japan Society of Ultrasound in Medicine.

1) M. Watanabe, K. Chihara, K. Shirae, K. Ishihara, and A. Kitabatake: *Proc. 11th Symp. Ultrasonic Electronics, Kyoto, 1990*, Jpn. J. Appl. Phys. **30** (1991) Suppl. 30-1, p. 241.
2) K. Okada, N. Kudo, K. Niwa, and K. Yamamoto: J. Med. Ultrason. **32** (2005) 3.
3) D. Koyama, A. Osaki, W. Kiyan, and Y. Watanabe: IEEE Trans. Ultrason. Ferroelectr. Freq. Control **53** (2006) 1314.
4) K. Ishihara, K. Yoshii, K. Chihara, K. Masuda, K. Shirae, and T. Furukawa: Proc. IEEE Ultrasonic Symp., 1992, p. 1277.
5) Y. Yamakoshi: Jpn. J. Appl. Phys. **40** (2001) 1526.
6) K. Wei, D. M. Skyba, C. Firschke, A. R. Jayaweera, K. R. Lindner, and S. Kaul: J. Am. Coll. Cardiol. **29** (1997) 1081.
7) K. Masuda, Y. Muramatsu, I. Mizobe, and K. Ishihara: Seitai Ikogaku **46** (2008) 275 [in Japanese].
8) H. Yoshikawa, T. Azuma, K. Sasaki, K. Kawabata, and S. Umemura: Jpn. J. Appl. Phys. **45** (2006) 4754.
9) H. Mitome: Jpn. J. Appl. Phys. **40** (2001) 3484.
10) Y. Yamakoshi and T. Miwa: Jpn. J. Appl. Phys. **47** (2008) 4127.
11) T. Kozuka, K. Yasui, T. Tuziuti, A. Towata, and Y. Iida: Jpn. J. Appl. Phys. **47** (2008) 4336.
12) T. Lilliehorn, U. Simu, M. Nilsson, M. Almqvist, T. Stepinski, T. Laurell, J. Nilsson, and S. Johansson: Ultrasonics **43** (2005) 293.
13) Y. Muramatsu, K. Masuda, S. Ueda, and K. Ishihara: Proc. 28th Ultrasonic Symp. 2007, p. 407.
14) Y. Muramatsu, S. Ueda, R. Nakamoto, Y. Nakayashiki, K. Masuda, and K. Ishihara: Proc. European Medical Biological Engineering Conf., 2008 p. 1589.

3P5-12

Proceedings of Symposium on Ultrasonic Electronics, Vol. 30 (2009) pp. 545-546
18-20 November, 2009

Evaluation of trapping performance of fluid microcapsules to the parameter variation in acoustic radiation

照射超音波のパラメータ変化に対する流路内マイクロカプセルの捕捉性能評価

Ryusuke Nakamoto[1‡], Hayato Yamauchi[1], Yusuke Muramatsu[1], Kohji Masuda[1], Yoshitaka Miyamoto[2], and Toshio Chiba[3]
([1] Tokyo Univ. Agri.& Tech.; [2] Nagoya Univ.; [3] National Center for Child Health and Develop.)
中元隆介[1‡], 山内勇人[1], 村松悠佑[1], 桝田晃司[1], 宮本義孝[2], 千葉敏雄[3]
([1]東京農工大学; [2]名古屋大学; [3]国立成育医療センター)

1. Introduction

Making use of the phenomena that microcapsules or microbubble of μm order collapse themselves after ultrasound emission near their resonant frequency, physical DDS (Drug Delivery System) has been proposed[1]. To minimize the side effect of medication, drug should affect to the target area, not to other parts inside human body. Though recent mainstream of DDS is focused on the gene transduction by using gene vector, it takes time and cost to develop for each object. The microcapsules, which can contain the specified drug inside the shell, have the possibility to correspond to various kinds of medications. However, because of the diffusion of capsules after injection, it was difficult to enhance the efficiency of medication. If the density of capsules inside human body can be controlled, the amount of drug would be minimum. Then we have noticed the acoustic radiation force [2], which is a physical phenomenon where an acoustic wave pushes an obstacle along its direction of propagation. When a microcapsule receives the acoustic radiation force against flow, it is trapped or propelled to the opposite direction of the flow. In this paper, we introduce our research to investigate local density of microcapsules in the straight artificial blood vessel according to the acoustic condition.

2. Principle

Fig.1 shows behavior of fluid microcapsules under acoustic emission. Considering the shape of a microcapsule as sphere, the acoustic radiation force F_{ac} acts to push the microcapsules to the direction of acoustic propagation[3]. On the other hand, when the microcapsules are put in flow, a capsule receives the flow resistant F_d. Thus, if F_d and F_{acx} in Fig.1 are similar, the acoustic radiation force balances with the flow resistant to trap fluid microcapsules.

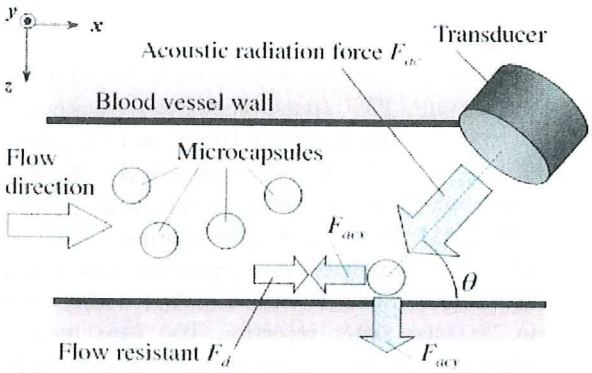

Fig.1 Behavior of fluid microcapsules under ultrasound emission.

3. Experiment

We used microcapsule F-04E (Matsumoto Oil, Japan) which shell is made of PVC (polyvinyl chloride) with specific gravity as 0.0225 and average of diameter as 3.5 [μm]. We sieved it as the range of diameter is 20 [μm] or less and the size is to be applied to use *in vivo*. Also we have prepared the artificial blood vessel, which is made of PEG (polyethylene glycol), including the straight vessel as **Fig.2**.

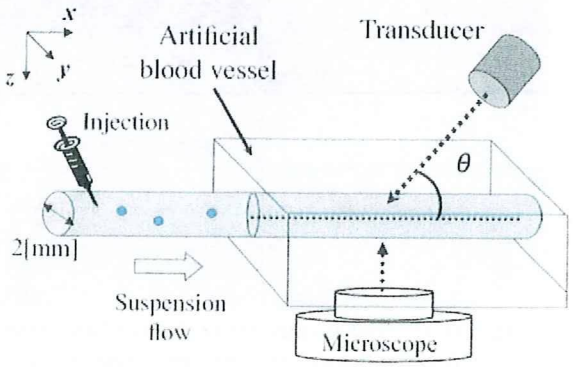

Fig.2 Schematic view of the experiment to trap fluid microcapsules

5000940315@st.tuat.ac.jp

The external size is 50x80x10 [mm] and inner diameter of the path is 2 [mm]. The transducer is set a direction of acoustic propagation to be opposite flow direction and θ = 45 [deg] to x-y plane as shown in **Fig.2**. We used a focal type transducer with center frequency of 1 [MHz] to emit ultrasound. We injected suspension of microcapsules with water of 0.3 [g/l] from upstream of the observed area, where focal point of ultrasound is included in the center. By using an optical microscope (KH-7700, Omron, Japan), behavior of microcapsules is observed and recorded.

4. Results

We produced several kinds of ultrasound waveform by varying PRF (pulse repetition frequency) and duty ratio, which ranged 10, 20 and 50 [kHz], and 40, 60, 80 and 100 [%], respectively. We adjusted maximum sound pressure at the focal point to be 300 [kPa]. **Fig.3** shows time series images of the observed area, when the suspension was injected by 20 [mm/s]. Injection was finished within 10 [sec]. In 20 [sec] after injection 100 [μm] order size aggregations of microcapsules were confirmed through thick suspension. The size of the aggregation saturated before 90 [sec]. As long as the behaviors of microcapsules were observed through the experiments, the reproducibility in shape, number and motion of the aggregation was poor. However, total occupied area of microcapsules was seemed to increase with the duty ratio, which indicates the amount of microcapsules increases in proportion to the duration of ultrasound emission.

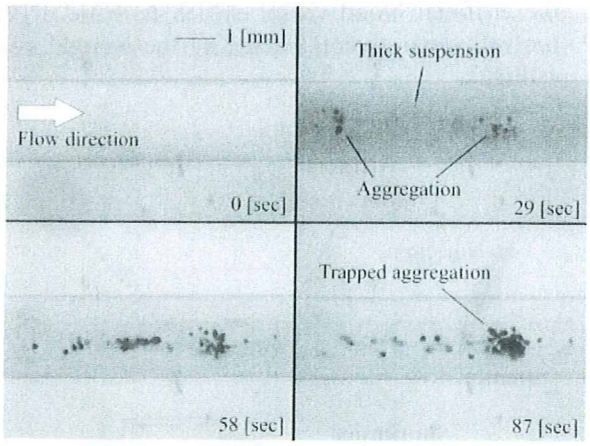

Fig.3 Time series images of the observed area after injection of the suspension with ultrasound emission.

To evaluate quantitative amount of trapped microcapsules, we measured the occupied area of microcapsules by labeling method. **Fig.4** shows the total occupied area of trapped microcapsules in 0~87 [sec] after ultrasound emission versus the duty ratio with PRF as a parameter. We confirmed the area increases according to duty ratio, where there was no significant difference in PRF variation. Therefore duration of ultrasound emission is important to trap microcapsules in flow. In many cases, aggregations of microcapsules were seen upstream before they were trapped, which should be caused by Bjerknes forces [1] produced by an ultrasound pressure gradient and oscillation of the diameter of the microcapsules. We consider that an aggregation of capsules makes equivalently a larger diameter capsule to receive more acoustic radiation force, which is proportional to the cube of the size of a microcapsule.

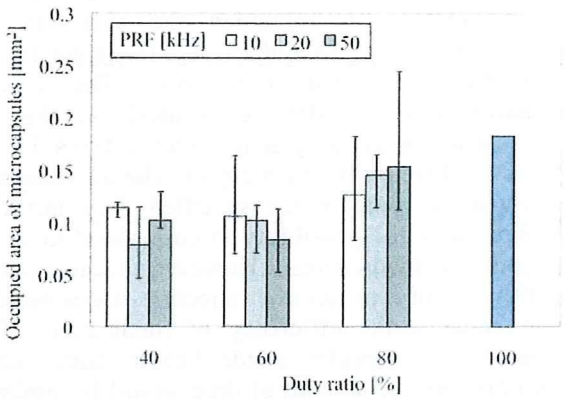

Fig.4 Occupied area of trapped microcapsules versus duty ratio of ultrasound

5. Conclusions

In this study, we have experimented to trap fluid microcapsules in artificial blood vessel. We confirmed the capsules with diameter of 3.5 [μm] were trapped in the middle of the path and by ultrasound of sinusoidal signal of 1 [MHz]. To trap capsules in flow, duration of ultrasound emission was important to make aggregation of capsules. We are going to apply the experiment by varying other parameters and to investigate the mechanism of the phenomena.

Acknowledgement

We would like to thank Dr. Teruyuki Kozuka for helpful suggestion and contribution of this research.

References

1) Y.Yamakoshi and T.Miwa, Jpn.J.Appl.Phys, 48 (2009) 07GK02
2) T.Kozuka et al., Jpn. J. Appl. Phys. 48 (2009) 07GM09
3) K.Masuda et al., Jpn. J. Appl. Phys. 48 (2009) 07GK03

3P5-3

Proceedings of Symposium on Ultrasonic Electronics, Vol. 30 (2009) pp. 529-530
18-20 November, 2009

Production of local acoustic radiation force to constrain microcapsules from diffusion in blood vessel

生体内マイクロカプセルの拡散抑制のための局所的音響放射力形成

Kohji Masuda[1], Nobuyuki Watarai[1], Ren Koda[2], Ryusuke Nakamoto[1], and Yusuke Muramatsu[1] ([1] Tokyo Univ. Agri.& Tech.; [2] Chiba Univ.)
桝田晃司[1], 渡會展之[1]、江田廉[2]、中元隆介[1]、村松悠佑[1], ([1]東京農工大; [2]千葉大)

1. Introduction

Microcapsules or microbubbles collapse upon exposure to ultrasound near their resonance frequency. The phenomenon has been identified as a basic method for drug delivery [1,2]. Making use of sonoporation [3], the existence of capsules (or bubbles) improves the introduction efficiency to affect the target area. While the lifetime of the microbubbles is several minutes, the microcapsules are thought to be better for use with various types of delivery. However, because of the diffusion of capsules after injection, it is difficult to deliver capsules to desired target area. If the behavior of capsules could be controlled, the introduction efficiency would be enhanced. Then we have ever reported our attempt to propel microcapsules in water owing to an acoustic radiation force [4,5], which is a physical phenomenon where an acoustic wave pushes an obstacle along its direction of propagation. We have elucidated the conditions in sound pressure, flow velocity and diameter of capsules for active path selection of capsules in an artificial blood vessel [6]. Then we have used the diameters of capsules ranged from 65 to 73 μm, which size is not to be applied *in vivo*. Considering that an acoustic radiation force is proportional to the cube of the size of a capsule, we have investigated with plane wave of ultrasound and smaller size of capsules for active path selection.

2. Theory

Assuming spherical capsules or bubbles, an acoustic radiation force [10] acts to propel the capsules in the direction of acoustic propagation as per the following equation,

$$F_{ac} = \frac{4}{3}\pi R_0^{\,3} A \frac{P^2}{\rho c^2}, \qquad (1)$$

where R_0 is the average capsule radius, P is the sound pressure, and r is the density of the medium. A is a constant which is derived from ρ and the density of capsules.

When the microcapsules are placed in flow, a capsule should receive a flow resistance F_d. If the acoustic radiation force is greater than the flow resistance, the trajectory of the capsule is curved, as shown in Fig.1.

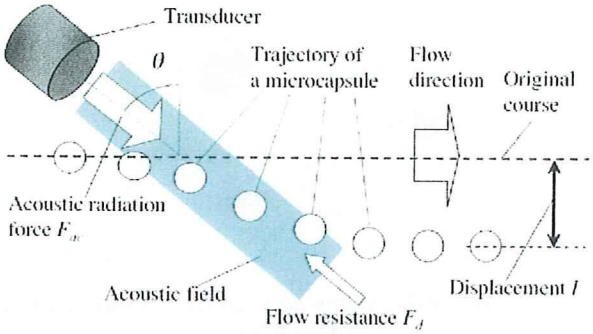

Fig.1. Trajectory of microcapsule in flow under ultrasound emission.

At larger value of angle θ in Fig.1, a capsule passes through the acoustic field for a longer period causing a larger displacement from the original course. In Fig.1, although the shape of the acoustic field is expressed as a square, it is measured before the calculation of theoretical displacement.

3. Experiment

We used the F-04E microcapsule, which has a shell made of polyvinyl chloride (PVC), a specific gravity of 0.0225, and an average diameter of 4 μm. It contains isobutene inside and is stable in room temperature. We selected only those microcapsules with a diameter less than 20 μm. We also have prepared an artificial blood vessel made of polyethylene glycol (PEG), including a Y-form bifurcation with inner diameter of the paths was 2 mm. The blood vessel was placed in the bottom of a water tank, which was filled with water. As shown in Fig.2, the observed area was recorded optically using an inverted microscope (Leica, DMRIB).

In Fig.2, the relationship between focal areas of ultrasound and the bifurcation is shown. The axis of

Kohji Masuda, e-mail: masuda_k@cc.tuat.ac.jp

the transducer was set at 40 degrees to the x-axis and θ deg to the z-axis to prevent physical interference between the transducer and the edge of the water tank. The transducer included a flat ceramic disc with a diameter of 25 mm to emit plane wave of ultrasound.

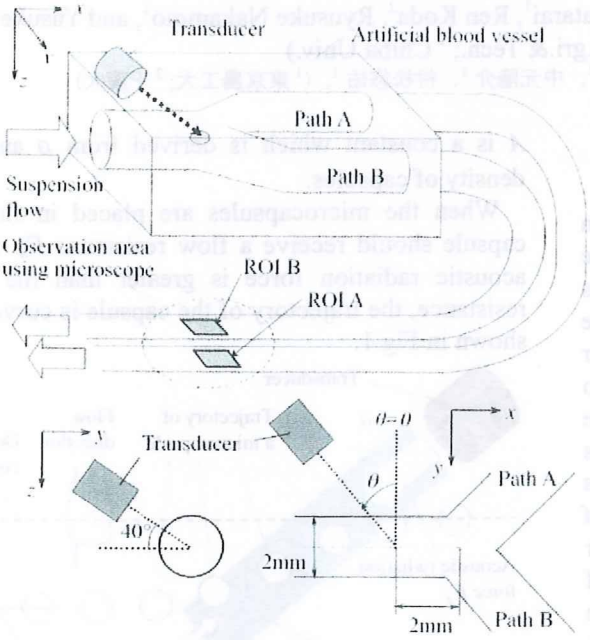

Fig.2. Relationship between focal points of ultrasound and the bifurcation area.

4. Result

When ultrasound was emitted, more capsules entered path B than path A, whereas no significant difference was observed without ultrasound emission. To evaluate the amount of capsules that passed through each path, we extended the two paths using semitransparent tubes and established the observed area, where both paths were observable in a single view. To measure amount of microcapsules, we established two square regions of interest in each path (ROIs A and B) and calculated the average brightness. The brightness of a region decreases depending on the number of capsules present. Thus, we defined the shadow index σ using the following equation to determine the number of capsules in each ROI,

$$\sigma = \left(REF - \sum_x \sum_y f(x,y) \right) / REF \qquad (2)$$

where f is the brightness of the ROI and REF is the summation of brightness in the absence of capsules in the ROI.

We measured the shadow indices in two ROIs upon emission of sinusoidal ultrasound with a frequency of 0.5 and 2 MHz, and a flow velocity of 5, 10 and 20 mm/s. Fig.3 shows the ratio in shadow index of ROI B to the summation versus the sound pressure at the bifurcation, where θ was fixed as 45 degree. In Fig.3, a ratio more than 50% indicates that more capsules passed through path B than path A. When the frequency is 2MHz, clear capsule selection to path B was confirmed.

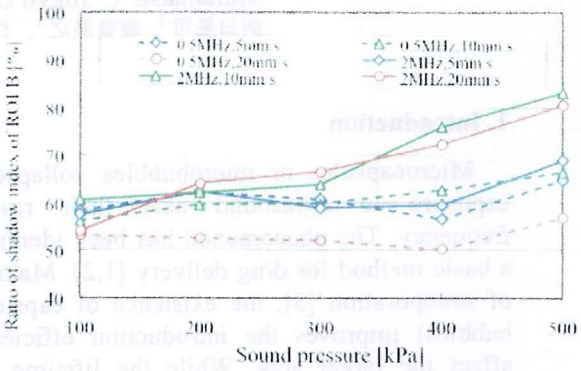

Fig.3. Ratio in shadow index of ROI B to the summation (ROI A and B) with $\theta = 45$ degree.

From the result, using higher sound pressure than 400kPa, 80% of capsules were introduced to a desired path, which result is much progressed than our previous attempt [6] using a focused ultrasound. For active path selection of capsules, higher pressure, higher frequency and plane ultrasound should be required.

5. Conclusion

In this study, we realized active control of microcapsules of micrometer size in an artificial blood vessel. We confirmed that capsules with a diameter less than 20 μm were directed into the desired path. For further analysis, the precise conditions necessary to realize active control of capsules in a complicated shape of blood vessel should be elucidated. Also we are going to apply to *in vivo* experiment.

Acknowledgment

This work was supported by Research and Development Committee Program of The Japan Society of Ultrasound in Medicine.

References

1. Y. Yamakoshi and T. Miwa: Jpn. J. Appl. Phys. 47 (2008) 4127-4131.
2. D.Koyama, et al.: Jpn. J. of Appl Phys, 43 (2004) 3215-3219.
3. K. Okada, et al.: J. Med. Ultrason. 32 (2005) 3-11.
4. T. Kozuka, et al.: Jpn. J. Appl. Phys. 47 (2008) 4336-4338.
5. T. Lilliehorn, et al.: Ultrasonics 43 (2005) 293-303.
6. K.Masuda, et al.: Jpn. J. Appl. Phys. 48 (2009) 07GK03

Study to trap fluid microcapsules in artificial blood vessel by producing local acoustic radiation force

Kohji Masuda[1], Ryusuke Nakamoto[1], Yusuke Muramatsu[1],
Yoshitaka Miyamoto[2], Keri Kim[3] and Toshio Chiba[3]

[1] Graduate School of Bio-Applications and Systems Engineering, Tokyo Univ. of Agri. &Tech., Tokyo, Japan
[2] School of Medicine, Nagoya University, Nagoya, Japan
[3] National Center for Child Health and Development, Tokyo, Japan

Abstract—**Microcapsules of μm order collapse themselves after ultrasound emission. Applying this technique as drug delivery system (DDS), not only local medication but also gene therapy method should be possible. However, it has been limitation to enhance the efficiency of medication because capsules suspension spreads in human body after the injection, where motion of capsules in blood flow cannot be controlled. To affect behavior of microcapsules, acoustic radiation force was introduced. We have observed the local aggregation of microcapsules by producing local acoustic radiation force in the artificial blood vessel. Then we estimated amount of trapped capsules by optical image processing. We confirmed fluid microcapsules of similar diameter with red blood cell were trapped in the middle of the path and by ultrasound of sinusoidal signal of 1 MHz. The condition to trap capsules was indicated by higher sound pressure and lower flow velocity.**

Keywords— **drug delivery system, microcapsule, acoustic radiation force, artificial blood vessel, trapping**

I. Introduction

Making use of the phenomena that microcapsules or microbubble of μm order collapse themselves after ultrasound emission near their resonant frequency, physical DDS (Drug Delivery System) has been proposed. To minimize the side effect of medication, drug should affect only to the target area, not to other parts inside human body. Though recent mainstream of research in DDS is focused on the gene transduction by using gene vector, it takes time and cost for development. The microcapsules, which can contain the specified drug inside the shell, have the possibility to correspond to various kinds of medications. Also the feature to use the microcapsules is easily detected and actuated by ultrasound. The distribution of capsules inside the body is easily recognized by echogram (B-mode image) because the brightness of echogram varies according to the density of capsules. However, because of the diffusion of capsules after injection, it was difficult to enhance the efficiency of medication. If the density of capsules inside human body can be controlled, the amount of drug would be minimum. Then we have noticed that microbubble aggregates in water by the effect of Bjerknes force [1,2] which is produced by pressure gradient of ultrasound and the oscillation of diameter in microbubble. Since the oscillation in microcapsule is smaller than in microbubble, because of the shell, a microcapsule is thought to receive the acoustic radiation force [3,4] to be pushed out with acoustic propagation. In this paper we describe our attempt [5,6] to trap fluid microcapsules in an artificial blood vessel by acoustic radiation force.

II. Method

Fig.1 shows behavior of fluid microcapsules under ultrasound emission. Considering the shape of a microcapsule as sphere, the acoustic radiation force F_{ac} acts to push the capsules to the direction of acoustic propagation. On the other hand, when the microcapsules are put in flow, a capsule should receive the flow resistant F_d. Thus, if F_d and F_{acx} in Fig.1 are similar, the acoustic radiation force balances with the flow resistant to trap fluid microcapsules.

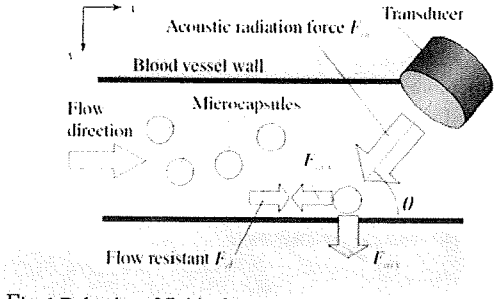

Fig. 1 Behavior of fluid microcapsules under ultrasound emission.

We used microcapsule F-04E which shell is made of PVC (polyvinyl chloride) with specific gravity as 0.0225 and average of diameter as 3.5 μm. We sieved it as the range of diameter is from 4 to 20 μm to be applied to use *in vivo*. We have prepared the artificial blood vessel, which is made of PEG (polyethylene glycol), including a straight path as the schematic view shown in Fig.2. The external size is 80 mm x 55 mm x 10 mm and the inner diameter of the path is 2 mm. It is placed in the bottom of water tank,

O. Dössel and W.C. Schlegel (Eds.): WC 2009, IFMBE Proceedings 25/VIII, pp. 206–207, 2009.
www.springerlink.com

which is filled with water. By using an optical microscope (KH-7700, Omron, Japan), behavior of microcapsules is observed and recorded.

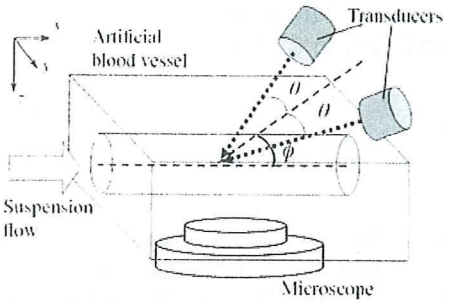

Fig. 2 Schematic view of the experiment to trap capsules.

We introduced two transducers to be focused at the same point with their angle and 2θ as shown in Fig.2. The plane which includes axes of the transducers is set $\phi = 50$ deg to prevent physical intervention between the transducer and an edge of the water tank. The transducer includes a concavity ceramic disc with the diameter of 25 mm. Ultrasound is emitted by amplifying sinusoidal signal to the amplitude 210 kPa where the focal area of ultrasound is created in 60 mm from the surface of the transducer with the half width of sound pressure in 8 mm.

III. Results

We observed the focused area under emission of sinusoidal ultrasound with frequency as 1 MHz, flow velocity as 20 mm/s and angle θ as 30 deg. Fig.3 shows time series microscopic images of the area where capsules are trapped in the middle of the path. Thus we confirmed the possibility to trap fluid microcapsules which sizes are similar to red blood cell under ultrasound emission.

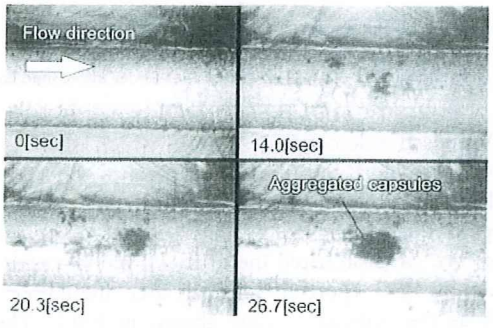

Fig. 3 Time series microscopic images where fluid microcapsules are trapped at the focused area under ultrasound emission (210kPa, 1MHz)

Then we measured amount of trapped capsules by calculating occupied area by capsules in the microscopic images when the amount of capsules is saturated. We experimented in various flow velocities and sound pressures. Fig.4 shows the occupied area by capsules versus flow velocity with parameter of sound pressure. When sound pressure is increased, much more amount of capsules was trapped. In the same sound pressure, the amount of capsules in 10 mm/s was more than in 20 mm/s.

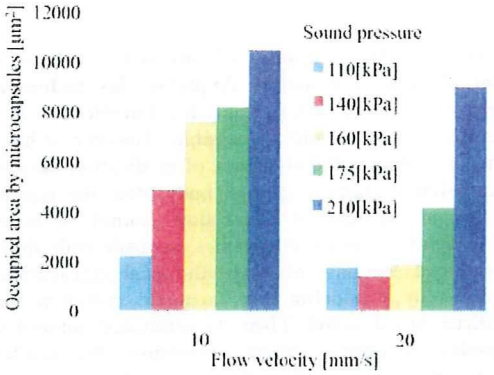

Fig. 4 Occupied area by microcapsules in the microscopic images versus flow velocity with parameter of sound pressure.

IV. Conclusions

In this study, we have experimented to trap fluid microcapsules in artificial blood vessel. We confirmed the capsules with diameter of 3.5 μm were trapped in the middle of the path and by ultrasound of sinusoidal signal of 1 MHz. The condition to trap capsules was indicated by higher sound pressure and lower flow velocity. We are going to apply the experiment by varying other parameters and to investigate the mechanism of the phenomena.

References

1. H. Mitome: Japanese Journal of Applied Physics, Vol.40 (2001) pp.3484-3487.
2. T. Lilliehorn, U. Simu, M. Nilsson, M. Almqvist, T. Stepinski, T. Laurell, J. Nilsson and S. Johansson: Ultrasonics, Vol.43 (2005) pp.293-303.
3. Y. Yamakoshi and T. Miwa: Japanese Journal of Applied Physics, Vol.47 (2008) pp.4127-4131.
4. T. Kozuka, K. Yasui, T. Tuziuti, A. Towata and Y. Iida: Japanese Journal of Applied Physics, Vol.47 (2008) pp.4336-4338.
5. Y. Muramatsu, S. Ueda, R. Nakamoto, Y. Nakayashiki, K. Masuda and K. Ishihara: Proc. of Euro. Med. & Biol. Eng. Conf. (2008) pp.1589-1593.
6. K.Masuda, Y.Muramatsu, S.Ueda, R.Nakamoto, Y.Nakayashiki and K.Ishihara: Japanese Journal of Applied Physics, Vol.48 (2009) in press

31st Annual International Conference of the IEEE EMBS
Minneapolis, Minnesota, USA, September 2-6, 2009

Active Control of Microcapsules in Artificial Blood Vessel by producing Local Acoustic Radiation Force

Kohji Masuda, *Member, IEEE*, Ryusuke Nakamoto, Yusuke Muramatsu, Yoshitaka Miyamoto, Keri Kim and Toshio Chiba

Abstract— **Micrometer-sized microcapsules collapse upon exposure to ultrasound. Use of this phenomenon for a drug delivery system (DDS), not only for local delivery of medication but also for gene therapy, should be possible. However, enhancing the efficiency of medication is limited because capsules in suspension diffuse in the human body after injection, since the motion of capsules in blood flow cannot be controlled. To control the behavior of microcapsules, acoustic radiation force was introduced. We detected local changes in microcapsule density by producing acoustic radiation force in an artificial blood vessel. Furthermore, we theoretically estimated the conditions required for active path selection of capsules at a bifurcation point in the artificial blood vessel. We observed the difference in capsule density at both in the bifurcation point and in alternative paths downstream of the bifurcation point for different the acoustic radiation forces. Also we confirmed the microcapsules are trapped against flow with the condition when the acoustic radiation force is more than fluid resistance of the capsules. The possibility of controlling capsule flow towards a specific point in a blood vessel was demonstrated.**

I. Introduction

THE phenomenon that microcapsules or microbubbles of micrometer size collapse upon exposure to ultrasound near their resonance frequency has been identified as a basis for a physical drug delivery system (DDS) [1-3]. To minimize side effects, medication should only affect the target area, not other parts of the human body. Although the majority of its recent research on DDSs has been focused on gene transduction using gene vectors, this method takes time and development is costly. While the lifetime of the microbubbles is several minutes, the microcapsules, which can contain a specific drug inside a shell, are suitable for use with various types of medication. Furthermore, microcapsules are easily detected [4] and actuated [5,6] by ultrasound. The distribution of capsules inside the body is easily determined by echogram (B-mode image) because the brightness of an echogram varies depending on capsule density. We have developed software to detect local changes in capsule density using the variation in brightness of an echogram [7]. Figure 1 shows a microscope image of F-80E microcapsules (Matsumoto Oil), which we used in this work.

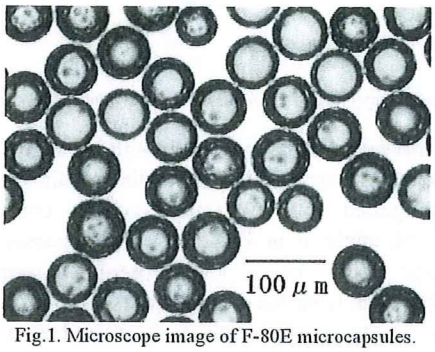

Fig.1. Microscope image of F-80E microcapsules.

However, because of the diffusion of capsules after injection, it is difficult to enhance the efficiency of medication. If the behavior of capsules could be controlled, the amount of medication required would be minimized. Microbubbles aggregate in water owing to Bjerknes forces, [8,9] which are produced by an ultrasound pressure gradient and oscillation of the diameter of the microbubbles. Since the oscillation of microcapsules is smaller than that of microbubbles, because of the microcapsule shell, a microcapsule is thought to receive an acoustic radiation force [10-12] and be propelled by acoustic propagation. In this paper, we describe our attempt for active path selection of microcapsules in an artificial blood vessel by acoustic radiation force.

II. Theory

Assuming spherical microcapsules, an acoustic radiation force [10] acts to propel the capsules in the direction of acoustic propagation as per the following equation:

$$F_{ac} = \frac{4}{3}\pi R_0^{\,3} A \frac{P^2}{\rho c^2}, \qquad (1)$$

where R_0 is the average capsule radius, P is the sound pressure, and ρ is the density of the medium. A is a constant which is derived from ρ and the density of capsules.

When the microcapsules are placed in flow, a capsule should receive a flow resistance F_d as per the following equation:

$$F_d = 6\pi R_0 \mu u_r, \qquad (2)$$

Manuscript received April 7, 2009. This work was supported in part by Health Labor Sciences Research Grant 200813004A.

Kohji Masuda, Ryusuke Nakamoto and Yusuke Muramatsu are with Graduate School of Bio-Applications and Systems Engineering, Tokyo University of Agriculture and Technology, Koganei, Tokyo, 184-8588 Japan (e-mail: masuda_k@cc.tuat.ac.jp).

Yoshitaka Miyamoto is with School of Medicine, Nagoya University, Nagoya, 466-8550 Japan.

Keri Kim and Toshio Chiba is with National Center for Child Health and Development, Tokyo, 157-8535 Japan

978-1-4244-3296-7/09/$25.00 ©2009 IEEE

where u_r is the velocity caused by the acoustic radiation force and μ is the viscosity coefficient of the medium. Thus, if ultrasound is directed at a microcapsule in flow, and the acoustic radiation force is greater than the flow resistance, the trajectory of the capsule is curved, as shown in Fig.2.

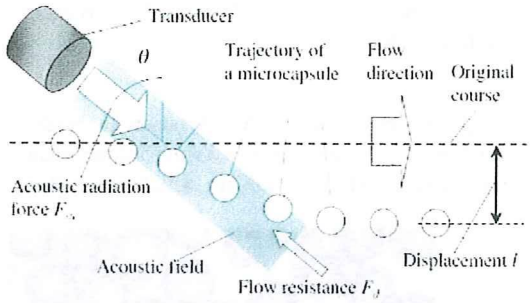

Fig.2. Trajectory of microcapsule in flow under ultrasound emission.

When microcapsules pass through an acoustic field where the sound pressure is higher than that at other areas, capsules are propelled away from their original course. At larger value of angle θ in Fig.2, a capsule passes through the acoustic field for a longer period causing a larger displacement from the original course. In Fig.2, although the shape of the acoustic field is expressed as a square, it is dependent upon the transducer and should be measured before the calculation of theoretical displacement.

III. Experiments

A. *Evaluation of active path selection of microcapsules*

We used the above-mentioned F-80E microcapsule, which has a shell made of polyvinyl chloride (PVC), a specific gravity of 0.0225, and an average diameter of 99.2 μm. It contains isobutene inside and is stable in room temperature. We selected only those microcapsules with a diameter in the range from 65 to 73 μm because of the limited magnification of the microscope. This size of capsule, of course, is not suitable for use *in vivo*, but is useful for confirming the fundamental behavior of capsules before minimizing them in the future experiments.

We also have prepared an artificial blood vessel made of polyethylene glycol (PEG), including a Y-form bifurcation as shown in the schematic view of Fig.3. The external size was 50 x 80 x 10 mm^3 and the inner diameter of the paths was 2 mm. The blood vessel was placed in the bottom of a water tank, which was filled with water. Because the acoustic impedance of PEG is similar to that of water, the energy of ultrasound in water reaches the path with high efficiency. Using an inverted microscope (Leica, DMRIB), optical images of the observed areas 1 and 2 indicated in Fig.3 were recorded independently.

Figure 4 shows the relationship between focal areas of ultrasound and the bifurcation in the observed area 1. The axis of the transducer was set at 50 degrees counterclockwise to the x-axis and θ deg clockwise to the z-axis to prevent physical interference between the transducer and the edge of the water tank. The transducer included a concave ceramic disc with a diameter of 25 mm. Ultrasound was emitted by amplifying a sinusoidal signal of 1 MHz to an amplitude of 160 kPa where the focal area of ultrasound is created in 60 mm from the surface of the transducer with a half width of sound pressure of 8 mm.

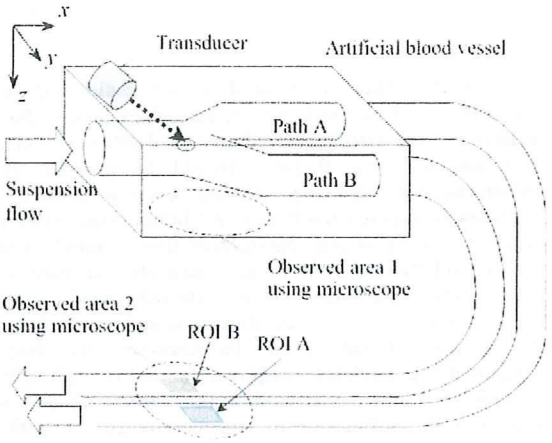

Fig.3. Configuration of artificial blood vessel, transducer, and two observed areas using microscope to evaluate active path selection of microcapsules.

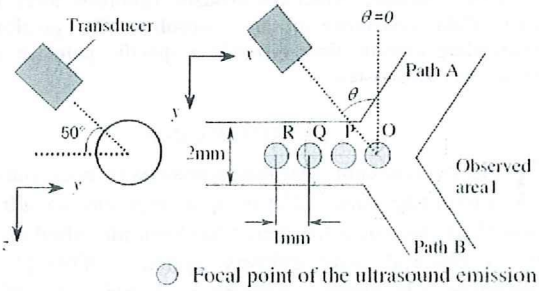

Fig.4. Relationship between focal points of ultrasound and the bifurcation in the observed area 1.

Defining point O as the intersection of the three paths in Fig.4, the points P, Q, and R indicate points 1, 2, and 3 mm upstream from O, respectively. We observed the behavior of capsules in the observed area 1 upon the injection of a capsule suspension at a flow velocity of 100 mm/s. When ultrasound was emitted, more capsules entered path B than path A, whereas no significant difference was observed without ultrasound emission. Figure 5 shows the comparison of microscope images of the observed area 1 before and after the capsule suspension was injected and ultrasound was focused at point Q. Since amount of capsules were observed as a shadow, the possibility of active path selection of capsules was indicated. Here we confirmed that the capsules were not destroyed by the ultrasound since the frequency used was far from the resonance frequency of the capsules.

To evaluate the number of capsules that passed through each path, we extended the two paths using semitransparent tubes and established an observed area 2, where both paths were observable in a single view, as shown in Fig.3.

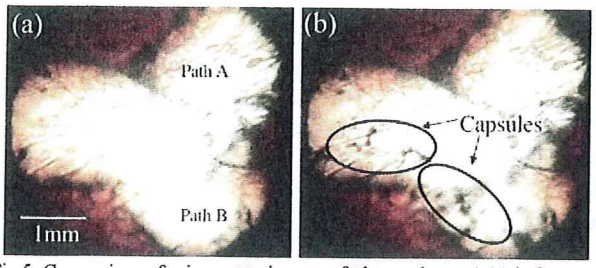

Fig.5. Comparison of microscope images of observed area 1 (a) before and (b) after injection of capsule suspension with ultrasound emission.

Figure 6 shows microscope images of the observed area 2, which were captured using a high-speed camera Phantom-V4.2 (Nobitec Co., Ltd., Japan) with an interval time of 2 ms, upon injection of a capsule suspension under the same conditions as for Fig.5. Individual microcapsules can be distinguished.

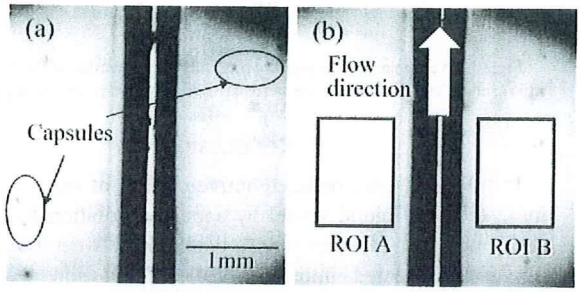

Fig.6. Microscope images of observed area 2 taken at 500 fps after injection of capsule suspension (a) without and (b) with ultrasound emission.

To measure the number of microcapsules, we established two square regions of interest in each path (ROIs A and B) and calculated the average brightness. The brightness of a region decreases depending on the number of capsules present. Thus, we defined the shadow index σ using the following equation to determine the number of capsules in each ROI:

$$\sigma = \left(REF - \sum_x \sum_y f(x,y) \right) / REF, \qquad (3)$$

where f is the brightness of the ROI and REF is the summation of brightness in the absence of capsules in the ROI. Then, we confirmed the relation between shadow index and capsule density. A capsule suspension was passed through the ROI without ultrasound and the average of the shadow index for 15 frames (duration 30 ms) was calculated for various flow velocities. When capsule density was 0.15-0.25 g/L, significant changes in density were detected [13].

B. Trapping microcapsules against flow

To observe the behavior of microcapsules if the acoustic radiation force propels microcapsules against flow, we have prepared the artificial blood vessel including a straight path as the schematic view, as shown in Fig.7. The external size is 55 x 80 x 10 mm^3 and the inner diameter of the path is 2 mm. It is placed in the bottom of water tank, which is filled with water. By using an optical microscope (KH-7700, Omron, Japan), behavior of microcapsules is observed and recorded.

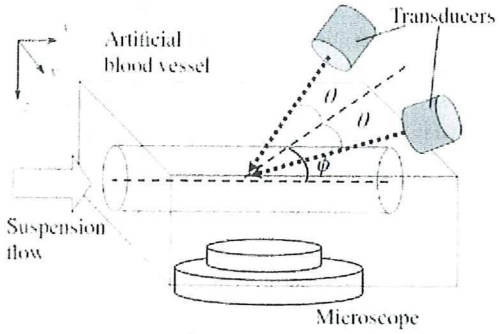

Fig. 7. Schematic view of the experiment to trap capsules.

We introduced two transducers, which were the same used for active path selection, to be focused at the identical point with their angle and 2θ as shown in Fig.7. The plane which includes axes of the transducers was set ϕ = 50 deg to prevent physical intervention between the transducer and an edge of the water tank. Ultrasound was emitted by amplifying sinusoidal signal to the amplitude from 110 to 210 kPa.

We observed the focal area under emission of sinusoidal ultrasound with frequency of 1 MHz and angle θ of 30 deg. Fig.8 shows a microscope image of the area where capsules are trapped by ultrasound of 175 kPa in the middle of the path against flow of 40 mm/s. Thus we established the ROI of 3.2 x 1.6 mm^2 in the image to measure occupied area by trapped microcapsules, which was similar evaluation to the above-mentioned shadow index.

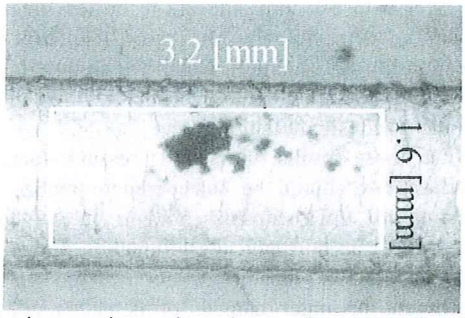

Fig. 8. A microscope image where microcapsules are trapped against flow at the focused area under ultrasound emission (210kPa, 1MHz)

IV. Results

A. Evaluation of active path selection of microcapsules

We measured the shadow indices in two ROIs upon emission of sinusoidal ultrasound with a frequency of 1 MHz, a flow velocity of 100 mm/s, and a capsule density of 0.2 g/L, where ultrasound was focused at points O, P, Q, and R shown in Fig.4. Figure 9 shows the difference in shadow indices between ROIs A and B versus the angle of

ultrasound emission θ for four focal points. Because the difference was calculated by subtracting the shadow index of ROI A from that of ROI B, a positive value for the difference indicates that more capsules passed through path B than path A. When the focal point was at O, no significant difference was observed. Upstream from O, clear capsule selection to path B was confirmed at angles of emission between 30 and 60 degrees. The optimum condition for active path selection in the experiment was at an angle of 50 degrees at focal point Q.

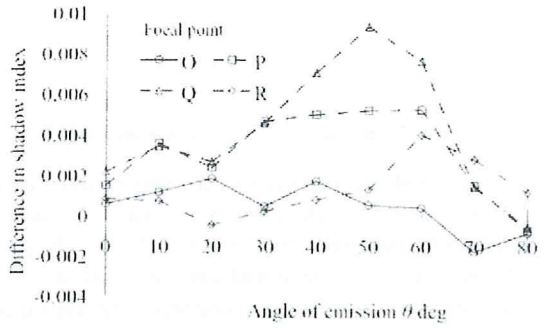

Fig.9. Shadow index difference between two ROIs versus angle of emission with ultrasound of 1 MHz, 160 kPa, and flow velocity of 100 mm/s.

We repeated the same experiment at a flow velocity of 100 mm/s. When the sound pressure was less than 120 kPa, there was no difference between the two ROIs. However, the value of shadow index in ROI B increased in proportion to the sound pressure at more than 140 kPa. More than 90% of capsules entered to path B when the sound pressure was more than 160 kPa. Next, when we fixed the sound pressure to 160 kPa, the value of shadow index in path B decreased in proportion to the flow velocity. The range of flow velocity for clear path selection appears to be less than 150 mm/s. When the flow velocity was more than 200 mm/s, path selection did not function, which we assume is because the capsules pass through the acoustic field without receiving sufficient acoustic radiation force.

From these results, the sound pressure, focal point, and flow velocity should be considered to realize active path selection of microcapsules. When the focal point of ultrasound emission is at the bifurcation point itself, active path selection of capsules is not realized. In the present experiment, the inner diameter of the path was 2 mm, so a 1 mm displacement was necessary from the beginning of the acoustic field to the bifurcation point, as shown in Fig.2.

B. *Trapping microcapsules against flow*

By referring the above condition, we recorded the microscope image when the amount of capsules is saturated under ultrasound emission. Then we calculated the average area occupied by trapped microcapsules in the ROI through the experiment. We attempted the experiment in various flow velocities and sound pressures. Fig.10 shows the average area occupied by microcapsules versus flow velocity with parameter of sound pressure. We confirmed the similar tendency of the active path selection when the flow velocity was fixed and the sound pressure was increased, average area occupied by microcapsules was increased. If the sound pressure was fixed, the average area was decreased in proportion to the flow velocity.

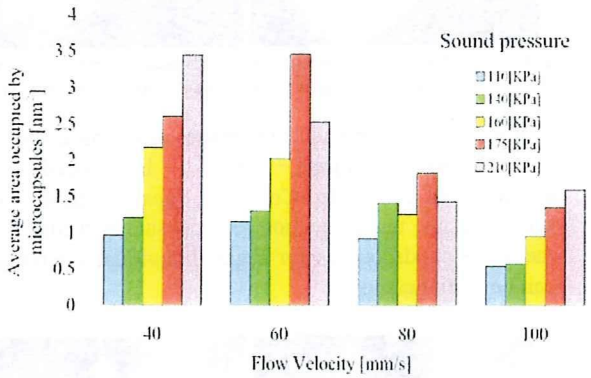

Fig.10. Average area occupied by trapped microcapsules in the ROI of microscopic image, versus flow velocity with parameters of sound pressure.

V. Conclusions

In this study, we realized active control of microcapsules in an artificial blood vessel by acoustic radiation force. We confirmed that capsules with a diameter between 65 and 73 μm were directed into the desired path and were not destroyed by ultrasound of a sinusoidal signal of 1 MHz. Also we confirmed that capsules were trapped against flow when the flow velocity was less than that the active path selection was observed. We are going to continue our research by varying other parameters of this experiment before applying *in vivo* experiment. For further analysis, the precise conditions necessary to realize active control of capsules in a complicated shape of blood vessel should be elucidated.

References

[1] M. Watanabe, K. Chihara, K. Shirae, K. Ishihara, and A. Kitabatake: Jpn. J. Appl. Phys. 30, (1991) Suppl.1, 241-243.
[2] K. Okada, N. Kudo, K. Niwa, and K. Yamamoto: J. Med. Ultrason. 32 (2005) 3-11.
[3] D. Koyama, A. Osaki, W. Kiyan, and Y. Watanabe: IEEE Trans. Ultrason. Ferroelect. Freq. Control, 53 (2006) 1314-1321.
[4] K. Ishihara, K. Yoshii, K. Chihara, K. Masuda, K. Shirae, and T. Furukawa: Proc. IEEE Ultrasonic Symp., 1992, p.1277-1280.
[5] Y. Yamakoshi: Jpn. J. Appl. Phys. 40 (2001) 1526-1527.
[6] K. Wei, D. M. Skyba, C. Firschke, A. R. Jayaweera, K. R. Lindner, and S. Kaul: J. Am. Coll. Cardiol., 29 (1997) 1081-1088.
[7] H. Yoshikawa, T. Azuma, K. Sasaki, K. Kawabata, and S. Umemura: Jpn. J. Appl. Phys. 45 (2006) 4754-4760.
[8] H. Mitome: Jpn. J. Appl. Phys. 40 (2001) 3484-3487.
[9] Y. Yamakoshi and T. Miwa: Jpn. J. Appl. Phys. 47 (2008) 4127-4131.
[10] T. Kozuka, K. Yasui, T. Tuziuti, A. Towata, and Y. Iida: Jpn. J. Appl. Phys. 47 (2008) 4336-4338.
[11] T. Lilliehorn, U. Simu, M. Nilsson, M. Almqvist, T. Stepinski, T. Laurell, J. Nilsson, and S. Johansson: Ultrasonics 43 (2005) 293-303.
[12] H.Zheng, P.A.Dayton, C.Caskey, S.Zhao, S.Qin and K.W.Ferrara : Ultrasound in Medicine and Biology, 33 (2007) 1978-1987
[13] K.Masuda, Y.Muramatsu, R.Nakamoto, S.Ueda, Y.Nakayashiki, and K.Ishihara: Jpn. J. Appl. Phys. 48 (2009) in press.